PHYSICAL REVIEW B **92**, 115148 (2015)

Discretized Abelian Chern-Simons gauge theory on arbitrary graphs

Kai Sun,[1] Krishna Kumar,[2] and Eduardo Fradkin[2]

[1]*Department of Physics, University of Michigan, 450 Church Street, Ann Arbor, Michigan 48109, USA*

[2]*Department of Physics and Institute for Condensed Matter Theory, University of Illinois at Urbana-Champaign, 1110 West Green Street, Urbana, Illinois 61801, USA*

(Received 2 February 2015; published 28 September 2015)

In this paper, we show how to discretize the Abelian Chern-Simons gauge theory on generic planar lattices/graphs (with or without translational symmetries) embedded in arbitrary two-dimensional closed orientable manifolds. We find that, as long as a one-to-one correspondence between vertices and faces can be defined on the graph such that each face is paired up with a neighboring vertex (and vice versa), a discretized Abelian Chern-Simons theory can be constructed consistently. We further verify that all the essential properties of the Chern-Simons gauge theory are preserved in the discretized setup. In addition, we find that the existence of such a one-to-one correspondence is not only a sufficient condition for discretizing a Chern-Simons gauge theory but, for the discretized theory to be nonsingular and to preserve some key properties of the topological field theory, this correspondence is also a necessary one. A specific example will then be provided, in which we discretize the Abelian Chern-Simons gauge theory on a tetrahedron.

DOI: 10.1103/PhysRevB.92.115148 PACS number(s): 11.15.Yc, 75.10.Kt, 73.43.−f, 05.30.Pr

I. INTRODUCTION

As the prototypical topological field theory, the Chern-Simons gauge theory has had a deep and broad impact on a wide range of physics research, ranging from knot theory [1] and parity anomalies in quantum field theory [2] to the theory of the integer and fractional quantum Hall effects [3–5] and the effective field theory description of chiral spin liquids [6,7] in condensed matter physics (for a review see, e.g., Ref. [8]). Although well understood as a continuum field theory, there is still limited understanding on how to discretize this topological field theory on two-dimensional (2D) lattices or graphs [9]. This task turns out to be highly nontrivial. In particular, the topological and gauge-theoretic nature of the Chern-Simons gauge theory enforces strong constraints on the dynamics of the gauge fields. These constraints, if not treated carefully, can result in inconsistencies in the discretized theory, making the theory ill defined [10,11]. Until recently, the discretization has been done only for a very special case, i.e., on a square lattice (with only nearest bonds) embedded in a torus [10,11]. It remains highly unclear as to whether similar construction can be extended for other lattices, or for lattices embedded on other 2D manifolds aside from the torus, or in any discretized systems without translation symmetries (e.g., a graph). In a recent publication [12], we presented a consistent construction of the Chern-Simons gauge theory on one of the simplest nonbipartite lattices in two dimensions, the kagome lattice, and used it to study the magnetizations plateaus of the spin-$\frac{1}{2}$ frustrated quantum Heisenberg antiferromagnet on this lattice.

The main purpose of this paper is to develop a consistent discretization of the Chern-Simons Abelian U(1) gauge theory on general planar lattices and graphs. There are several motivations to search for a discretized Chern-Simons gauge theory on generic lattices/graphs. For example, it has been known that the Chern-Simons gauge theory plays a crucial role in the study of chiral spin liquid. Such an exotic state of matter can only be stabilized in the presence of strong geometric frustration. Much of the work in frustrated antiferromagnets uses the fact that these systems are equivalent to a system of (generally interacting) hard-core bosons on the same lattice. The hard-core bosons are then mapped into a system of fermions coupled to a discretized Chern-Simons gauge field [9]. Except for some very special exactly solvable models, in the study of such frustrated systems the dynamics and quantum fluctuations of the effective gauge fields are typically ignored, and frustrated quantum antiferromagnets are frequently described only at the level of the average field approximation [13,14]. However, such an approximation is unreliable, and has a strong and obvious bias towards time-reveal breaking ground states. As shown in Ref. [15], to correctly address the competition between different quantum ground states, it is necessary to go beyond the average field approximation by carefully introducing the correct quantum dynamics.

It was recently realized that, in addition to the well-known case of two-dimensional electron gases (in the continuum) in strong magnetic fields, the fractional quantum Hall effect can also be stabilized in lattices even with zero net magnetic field [16–21]. Fractional quantum Hall states have also been explored on lattice systems earlier on [22,23] and, more recently, also in optical lattice systems [24–27]. This type of (discrete) fractional topological state is now often referred to as the fractional Chern insulators or the fractional quantum anomalous Hall state. In particular, it has been shown that these (discrete) fractional Chern insulators are adiabatically connected to the corresponding fractional quantum Hall states in the continuum [28–30].

The Chern-Simons gauge theory is known to be the low-energy, hydrodynamic, theory of topological phases such as the fractional quantum Hall fluids [5]; they are also expected to describe the low-energy and long-distance limit of topological Chern insulators, fractional or not [31–35]. Although Chern-Simons theories yield a natural description of the hydrodynamic behavior of topological phases, *a priori* they are not absolutely necessary in the microscopic construction of a theory of such states [5]. However, all known fractionalized phases are in inherently strongly coupled systems and, notably in the case of the fractional quantum Hall fluids, the use of

Chern-Simons gauge theory in the microscopic derivations has been invaluable [3,4]. Aside from some recent and promising work [36,37], it is not yet clear what role Chern-Simons gauge theory plays in the theory of fractional topological Chern insulators. Although adiabatic continuity strongly implies that the theory of factional Chern insulators should be smoothly related to the theory of the fractional Hall effect on lattice systems [22,23], where discrete Chern-Simons gauge theory is expected to be generally applicable, the general answer to these questions has remained problematic in view of the fact that the Chern-Simons gauge theory has not been discretized on most of the lattices on which lattice fractional Chern insulators are known to occur (e.g., the checkerboard lattice, the kagome lattice, and the multiple-orbital square lattice). Although we will not give an answer for systems on lattices as general as it is needed, we will give an explicit construction for a large class of lattices, which include some of clear physical interest.

In this paper, we propose and study a discretized Chern-Simons gauge theory on generic planar graphs embedded in arbitrary 2D closed and orientable manifolds [38]. Same as in a lattice gauge theory, we will define the space components of the gauge field to live on the nearest-neighbor bonds of the lattice and the time components on the sites (vertices) of the lattice. We will consider only planar lattices (and hence with only noncrossing bonds). This is a lattice gauge theory [39–42], but one with a broken time-reversal and parity invariance. Here, we will be interested in a version of Chern-Simons theory on a class of spatial lattices with continuous time. Earlier work focused on the square lattice [9–11,43], and recently we discussed the case of the kagome lattice [12]. Discretized versions of Chern-Simons gauge theory have been discussed both in Euclidean space-time lattices [44], which suffer from the species doubling problem analogous to those of lattice fermions. By enlarging the scope of investigation from periodic lattices to graphs (with or without translational symmetries), our conclusions are generally applicable for a wide range of systems.

We will require the discretized theory to retain the central features a topological field theory. Chern-Simons gauge theory on a continuous space-time manifold has several key features [1]. It is gauge theory which means that it has a local symmetry under local (in space-time) gauge transformations. At the quantum level, this requires that the quantum states of the physical Hilbert space be gauge invariant [45], and hence that the generators of local time-independent gauge transformations must generate superselection sectors, i.e., the Gauss law is satisfied as constraint on the physical space of states. For this requirement to be consistently implemented, the generators of local gauge transformations must commute with each other on different spatial locations. In the case of the Chern-Simons theory, this implies that the local magnetic flux must commute with each other (since they are the generator of time-independent gauge transformations). This condition imposes stringent constraints on the possible form of the discretized theories [10,11], and it is the main focus of this work.

On the other hand, at the classical level, the Chern-Simons theory is topological in the sense that the action is invariant under general coordinate transformations and hence it is independent of the metric. A consequence of this feature is

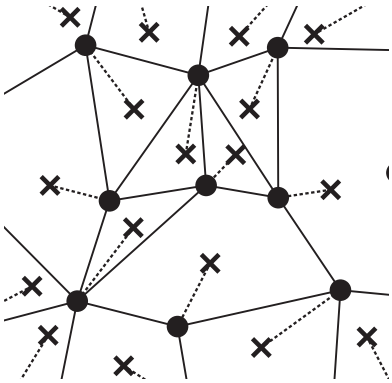

FIG. 1. Part of a planar graph, on which a local vertex-face correspondence is defined. The disks and solid lines represent vertices and edges of the graph, respectively. Each face is marked by a cross. The local vertex-face correspondence is indicated by dotted lines, that pair up each face with one (and only one) adjacent vertex.

that the energy-momentum tensor classically vanishes and, consequently, the Hamiltonian is also zero. Clearly, any lattice discretization implies a choice of coordinates, i.e., a fixed spatial metric. Furthermore, a change of the lattice stricture leads to a change in the form of the metric. Therefore, a lattice version of Chern-Simons theory cannot be explicitly independent of the metric and, in this sense, it cannot be formally topological. However, we will show in the following that one can construct a Chern-Simons gauge theory for a large class of lattices a U(1) lattice gauge theory with continuous time (i.e., in "Hamiltonian" form [40]) which is gauge invariant. We will see that the resulting discretized theory nevertheless has a vanishing Hamiltonian since the content of the action reduces to a set of (reasonably local) equal-time commutation relations and a set of local and commuting constraints. This theory is topological in the sense that it does not have local excitations, and that only the global degrees of freedom (nontrivial Wilson loops) matter. In the long-wavelength limit, the discretized theory becomes (formally) the continuum Chern-Simons gauge theory.

We find that such a Chern-Simons gauge theory can be constructed for arbitrary 2D planar graphs (lattices) as long as a *local vertex-face correspondence* can be defined on the graph/lattice. We adopt the following definition:

Definition. A local vertex-face correspondence is a one-to-one correspondence between faces and vertices defined on a graph such that every vertex is adjacent to its corresponding face (and vice versa).

An example of such a correspondence is shown in Fig. 1. The relevance of this correspondence to Chern-Simons theory lies in the nature of this gauge theory. In the continuum, the (Abelian) Chern-Simons Lagrangian of a gauge field $\mathcal{A}_\mu$ in 2+1 dimensions is (coupled to a matter current J_μ)

$$\mathcal{L}_{\rm CS}[\mathcal{A}] = \frac{k}{4\pi}\epsilon^{\mu\nu\lambda}\mathcal{A}_\mu\partial_\nu\mathcal{A}_\lambda - J_\mu\mathcal{A}^\mu. \tag{1.1}$$

The Chern-Simons (CS) gauge theory is a topological field theory [1]. At the classical level, the CS action is independent on the metric of the manifold on which it is defined. The content of this Lagrangian [Eq. (1.1)] is seen in Cartesian

components

$$\mathcal{L}_{\rm CS}[\mathcal{A}] = \frac{k}{2\pi}\mathcal{A}_0\mathcal{B} - J_0\mathcal{A}_0 - \frac{k}{4\pi}\epsilon_{ij}\mathcal{A}_i\partial_t\mathcal{A}_j - \boldsymbol{J}\cdot\boldsymbol{\mathcal{A}}. \quad (1.2)$$

At the quantum level, the first term of the right-hand side becomes the requirement that the states in the physical Hilbert space $\{|\text{Phys}\rangle\}$ obey the "Gauss law" as a local constraint. Thus, the physical states are gauge invariant and are annihilated by the generator of local gauge transformations

$$\left[\frac{k}{2\pi}\mathcal{B}(\boldsymbol{x}) - J_0(\boldsymbol{x})\right]|\text{Phys}\rangle = 0. \quad (1.3)$$

Hence, the physical states are those in which the local charge density J_0 and the local magnetic flux $\mathcal{B} = \epsilon_{ij}\partial_i\mathcal{A}_j$ are precisely related, i.e., flux attachment. The second term of the right-hand side of Eq. (1.2) implies that the components of the gauge field obey the equal-time commutation relations

$$[\mathcal{A}_i(\boldsymbol{x}),\mathcal{A}_j(\boldsymbol{y})] = i\frac{2\pi}{k}\epsilon_{ij}\delta(\boldsymbol{x}-\boldsymbol{y}). \quad (1.4)$$

Further, the Hamiltonian of this system is zero unless sources are present, i.e.,

$$\mathcal{H} = \boldsymbol{J}\cdot\boldsymbol{\mathcal{A}}, \quad (1.5)$$

which is a consequence that a topological field theory does not have any excited states with finite energy.

As with any lattice gauge theory, in a discretized Chern-Simons gauge theory the gauge fields (which are connections and hence are 1-forms) are naturally defined on the links of the lattice while the matter fields are defined on the sites of the lattice [39,40]. The field strength is a 2-form and it is defined on the elementary plaquettes of the lattice. While in a conventional lattice gauge theory the lattice is generally hypercubic (i.e., square in 2D), here we will consider more general (and translationally invariant) planar lattices. For instance, in Ref. [9] (and in Refs. [10,11]) the Chern-Simons theory was defined on a square lattice and in Ref. [12] the theory was defined on a kagome lattice. In both cases, the Gauss law of Eq. (1.3) is naturally implemented as a constraint that relates the occupation number of a site (or vertex) to the gauge flux through a (uniquely defined) adjoint plaquette (or face). While in the case of the square lattice all plaquettes are identical (squares), in the case of the kagome lattice has three inequivalent sites in its unit cell and, correspondingly, three faces (two triangles and a hexagon) in its unit cell. Nevertheless, the correspondence of vertices to faces is one-to-one in both lattices.

We will see here that this correspondence is a key feature which will allow us to impose the constraint (and hence gauge invariance) in a unique way which, in addition, does not break the point-group (or space-group) symmetries of the lattice. Following, we will find a construction of the Chern-Simons gauge theory on lattices for which for a charge located at a vertex, the magnetic field attached to it by the Chern-Simons gauge theory, is located at the face that is naturally paired up with this vertex.

Whether or not a local vertex-face correspondence can be defined for a graph is fully determined by the connectivity of the graph. In Sec. II, we will provide a sufficient and necessary condition, which can be used to decide whether such a correspondence exists or not for an arbitrary graph. In Fig. 2, we show some examples of lattices that support such a correspondence (i.e., a discretized Chern-Simons gauge theory can be constructed on these lattices). These examples include some of the lattices used in the study of chiral spin liquids and the lattice fractional quantum Hall effect (e.g., the kagome lattice).

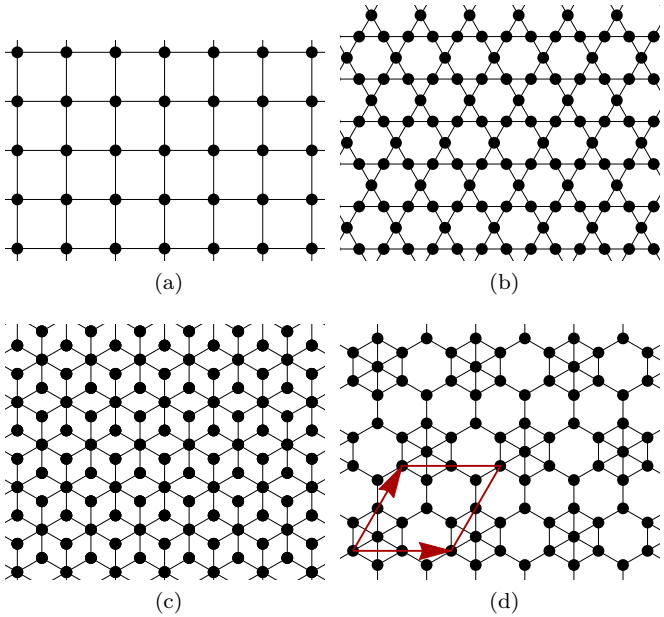

FIG. 2. (Color online) Examples of lattices and graphs that support local vertex-face correspondences. (a) A square lattice with 1 vertex and 1 face per unit cell, (b) a kagome lattice with 3 vertices and 3 faces per unit cell, (c) a dice lattice with 3 vertices and 3 faces per unit cell, and (d) a lattice that contains 9 vertices, 18 edges, and 9 faces per unit cell. The (red) parallelogram marks a unit cell with lattice vectors indicated by the two (red) arrows. It is easy to verify that for all these lattices $N_v = N_f$ and for any subgraphs the number of faces never exceeds the number of vertices, which is a sufficient and necessary condition for the existence of (at least) one local vertex-face correspondence.

It is also worthwhile to emphasize that in the continuum, the Chern-Simons gauge theory can be defined on arbitrary 2D closed and orientable manifolds. This plays a critical role in the phenomenon of topological degeneracy in fractional quantum Hall systems [46]. In addition, it is also known that all the essential physics of the Chern-Simons gauge theory (in the continuum) is stable against the explicit breaking of the translational symmetry, which is the underlying reason for the stability of the quantum Hall states against weak disorders. On the discretized side, however, it is still unclear whether the Chern-Simons gauge theory can be defined on any manifold aside from a torus and/or on a discrete graph without translational symmetries. Our study will provide an answer to these questions.

In addition to those geometric considerations, a key consistency requirement of the gauge theory is that the lattice version of the local constraints of Eq. (1.3) must commute with each other and hence act as superselection rules on the Hilbert space [10,11] (otherwise, these constraints cannot be simultaneously satisfied). This consistency condition places

restrictions on the commutation relations satisfied by the gauge fields defined on the links. For the square lattice, this problem was solved by Eliezer and Semenoff [10,11], and was more recently generalized by us to the case of the kagome lattice [12]. In this paper, we will show that the commutation relations can be defined consistently on any lattice (and graph) which obeys the one-to-one correspondence between vertices and faces. We will show that this restriction is implemented in terms of a suitably defined nonsingular (and hence invertible) matrix. Therefore, the lattice Chern-Simons theory can be defined as a consistent gauge theory at the quantum level on these planar lattices and graphs.

This paper is organized in the following way. In Sec. II, we present a necessary and sufficient criterion for determining whether a local vertex-face correspondence can be defined for an arbitrary graph/lattice. In Sec. III, we write the action of the discretized Chern-Simons gauge theory for generic graphs with a local vertex-face correspondence. In Secs. IV–IX, we prove that our discretized gauge theory preserves all key features of the Chern-Simons gauge theory, including the gauge invariance, flux attachment, commutation relations, duality transformation, and the locality condition. In Sec. X, we show that the existence of a local vertex-face correspondence is the necessary condition for discretizing the Chern-Simons theory, if we want the theory to be nonsingular and to preserve the key properties of the Chern-Simons gauge theory. In Sec. XI, we present a simple example by discretizing the Chern-Simons gauge theory on a tetrahedron, which is a 2D planar graph on a sphere. In Sec. XII, we conclude our paper by discussing open problems and applications of this theory to a number of systems of interest. Details of the calculations are presented in several appendixes.

II. LOCAL VERTEX-FACE CORRESPONDENCE

We start our discussion by presenting all constraints and assumptions that will be enforced on the graphs (and lattices) that we will consider. In this paper, we study generic *planar simple* graphs embedded on arbitrary closed and orientable 2D manifolds. Here, "planar" indicates that the graph can be drawn on a 2D manifold without any crossing bonds, while "simple" means no multiple bonds connecting the same pair of sites and no bond connecting a site to itself (see Fig. 11 in Appendix A for an explicit example). The "simple" condition is automatically implied for most (if not all) lattices studied in physics, while the "planar" condition holds for many (but not all) of them.

For a planar graph G, we can construct the dual graph G^* by mapping vertices to faces, and vice versa. Because, as will be discussed in the following, the dual graph will be needed for the dual gauge theory, we will also require the dual graph G^* to be *simple*. For the original graph G, this condition implies that G cannot contain any dangling bonds, and that two faces in G can share at most one common edge.

From now on, we will focus our study on graphs, on which a local vertex-face correspondence can be defined. In Sec. X, we will prove that this constraint is necessary in order to preserve certain key defining properties of the Chern-Simons gauge theory.

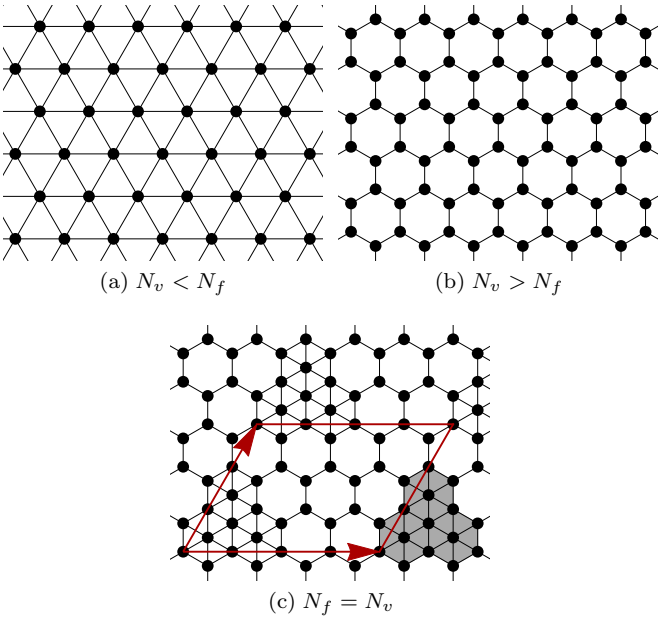

(a) $N_v < N_f$ (b) $N_v > N_f$ (c) $N_f = N_v$

FIG. 3. (Color online) Examples of lattices/graphs that do not support a local vertex-face correspondence. (a) A triangular lattice, which has 1 vertex and 2 faces per unit cell ($N_v < N_f$), (b) a honeycomb lattice, which has 2 vertices and 1 face per unit cell ($N_v > N_f$), and (c) a lattice with $N_v = N_f$ but some of the subgraph has more faces than vertices, e.g., the dark area, which has 18 faces and 16 vertices. The (red) parallelogram marks a unit cell with lattice vectors indicated by the two (red) arrows. Each unit cell of this lattice contains 27 vertices, 54 edges, and 27 faces ($N_v = N_f$).

To determine whether a graph can support such a local vertex-face correspondence, we will use the following criterion:

Criterion. A local vertex-face correspondence can be defined on a 2D planar graph G, if and only if the graph has the same number of vertices and faces (i.e., $N_v = N_f$), and that for any subgraph of G the number of faces never exceeds the number of vertices (i.e., $N'_v \geqslant N'_f$).

That this criterion is a sufficient and necessary condition is proved in Appendix B. The proof utilizes *Hall's marriage theorem* by mapping the local vertex-face correspondence to *Hall's marriage problem* [47]. The marriage theorem is named after the British mathematician, Philip Hall, who should not be confused with the physicist Edwin Hall, after whom the Hall effect is named.

Using this criterion it is straightforward to determine whether or not a graph or lattice can support a local vertex-face correspondence. In Fig. 2 (Fig. 3), we provide examples of lattices/graphs, on which such a local correspondence exists (does not exist). In Fig. 3, the first two lattices do not support any one-to-one correspondence between vertices and faces because the number of faces does not match the number of vertices. The third example, shown in Fig. 3(c), has the same number of faces and vertices and, thus, in principle, a one-to-one correspondence between vertices and faces could be defined. However, in this case such a correspondence cannot be local, as proven in Appendix B, because this lattice contains some subgraph, whose number of faces exceeds the number

of vertices. For example, the dark area in Fig. 3(c) shows a subgraph with 18 faces and 16 vertices.

In Figs. 2(b) and 2(c), the two lattices are dual to each other. Generically, if a graph G has a local vertex-face correspondence, so does its dual graph G^*. This is because one can construct such a correspondence for G^* by simply swapping the vertices and faces in the original vertex-face correspondence defined on G. As a result, our discretized Chern-Simons gauge theory always arises in pairs (one on the graph G and the other on the dual graph G^*). In Sec. VI, we will prove that these two gauge theories are dual to each other. This duality relation is different from the continuum, in which the Chern-Simons theory is self-dual. A discretized Chern-Simons gauge theory is in general not self-dual, unless the underlying graph is self-dual. One example of a self-dual graph is shown in Fig. 2(a), i.e., a square lattice. Another self-dual graph will be presented in Sec. XI, i.e., a tetrahedron.

We conclude this section by highlighting some conventions adopted in this paper. For a graph G, we label the numbers of vertices, edges, and faces as N_v, N_e, and N_f, respectively, and we use the subindices v, e, and, f to label each vertex, edge, and face, respectively, where v, e, and f take integer values ($1 \leqslant v \leqslant N_v$, $1 \leqslant e \leqslant N_e$, and $1 \leqslant f \leqslant N_f$). For the dual graph G^*, we will use the "$*$" symbol to label every object. For example, vertices, edges, and faces of the dual graph are labeled as v^*, e^*, and f^*, respectively. In addition, for convenience, if a vertex v in graph G is mapped to the face f^* in the dual graph, we will use the same integer to label them, i.e., $v = f^*$. Same is true for corresponding e and e^* (f and v^*). Throughout the paper, repeated indices will be summed over unless specified otherwise. For the gauge field, the time component lives on vertices and thus will be labeled as A_v. The spatial components (i.e., the vector potential) are defined on edges, and thus will be shown as A_e. Because the vector potential is a vector, we must choose a positive direction for each edge (from one of its ends to the other). The vector potential A_e on an edge e is positive (negative), if it is along (against) the direction of the edge e. In graph theory, after a direction is assigned to each edge, the graph is called a directed graph (or a digraph) [47].

III. DISCRETIZED CHERN-SIMONS ACTION

In this section, we construct the action of the discretized Chern-Simons gauge theory. We should emphasize that as long as the conditions discussed in the previous section are satisfied, our construction is applicable for arbitrary graphs.

A. The M matrix and the K matrix

In this section, we define two matrices for arbitrary graphs with a local vertex-face correspondence. For a graph satisfying the criterion given in the previous section, typically there is more than one way to define the local vertex-face correspondence, and different choices here will in general result in different M and K matrices and thus lead to slightly different actions. Here, we choose a specific (albeit arbitrary) one, consistently throughout the lattice.

The vertex-face correspondence defines a matrix $M_{v,f}$ with dimensions $N_v \times N_f$. The first index of this matrix runs over all vertices, while the second one indicates faces in the graph. If vertex v and face f are paired up according to the vertex-face correspondence, then $M_{v,f} = 1$. Otherwise, the matrix element is zero. Hence,

$$M_{v,f} = \begin{cases} 1 & \text{if } v \text{ is paired with } f, \\ 0 & \text{otherwise.} \end{cases} \tag{3.1}$$

Because the vertex-face correspondence requires $N_v = N_f$, the matrix M is a square matrix. In addition, it is easy to realize that, by definition, M is an invertible and orthogonal matrix, i.e., the inverse matrix M^{-1} is the transpose matrix $M^T = M^{-1}$.

In addition to M, the local vertex-face correspondence can be used to define another $N_e \times N_e$ square matrix, which we will denote by K, whose two indices run over all edges of the graph (with N_e being the number of edges):

$$K_{e,e'} = \begin{cases} \pm\frac{1}{2} & \text{if } e \text{ and } e' \text{ belongs to the same face,} \\ 0 & \text{otherwise.} \end{cases} \tag{3.2}$$

If there exists a face f such that e and e' are both edges of this face, the component of the matrix $K_{e,e'}$ is $\pm\frac{1}{2}$. Otherwise, the matrix element vanishes. For nonzero $K_{e,e'}$, the $\pm$ sign is determined by the following formula:

$$K_{e,e'} = -\frac{\eta_1 \times \eta_2}{2} = \pm\frac{1}{2}, \tag{3.3}$$

where $\eta_1 = \pm 1$ and $\eta_2 = \pm 1$ are two $\mathbb{Z}_2$ integers.

The sign of η_1 is determined using the following rule. As shown in Fig. 4, we first mark the vertex that is paired up with f in the local vertex-face correspondence using a (red) circle. After that, we go from the edge e to the edge e' by moving counterclockwise around the face f. If the path goes though the specially marked vertex (the red circle in Fig. 4), $\eta_1 = +1$, and otherwise $\eta_1 = -1$.

The sign of η_2 is determined by the directions of the two edges e and e'. As discussed above, to define the vector potential, we must specify the direction for each edge. When we go around the face f in the counterclockwise direction, if both e and e' are pointing along (or opposite to) the direction of the path, $\eta_2 = +1$. If one of them points along the path while the other is opposite, $\eta_2 = -1$.

With η_1 and η_2, their product (multiplied by -1) $-\eta_1 \times \eta_2 = \pm 1$ determines the sign of $K_{e,e'}$ in Eq. (3.2). Some examples can be found in Fig. 4.

B. Action

With the two matrices defined above, we can now write the action of our discretized Chern-Simons gauge theory:

$$S = \frac{k}{2\pi} \int dt \left[A_v M_{v,f} \Phi_f - \frac{1}{2} A_e K_{e,e'} \dot{A}_{e'} \right]. \tag{3.4}$$

Here, we sum over all repeated indices. The indices v, f, and e run over all vertices, faces, and edges, respectively. A_v is the time component of the gauge field, which lives on vertices and A_e represents the spatial components, which are defined on edges. Here, $\dot{A}$ represents the time derivative, K and M are the two matrices defined in the previous subsection, and Φ_f is the magnetic flux on the face f, which equals to the loop

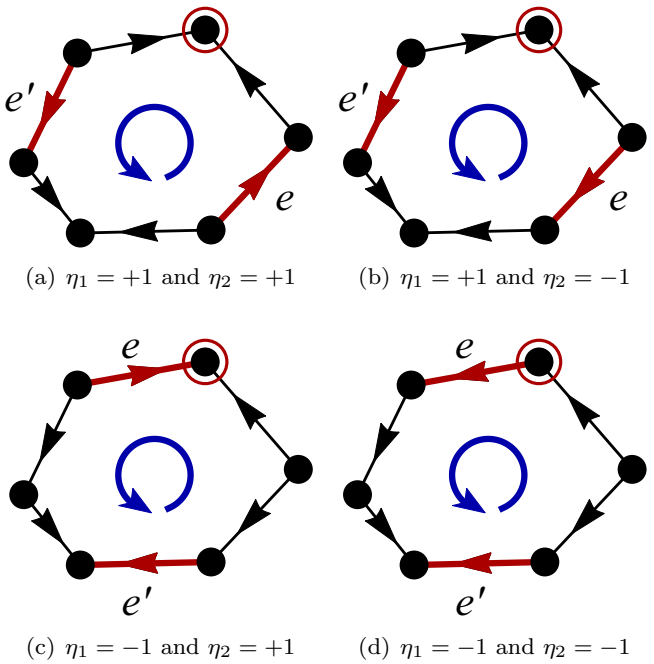

(a) $\eta_1 = +1$ and $\eta_2 = +1$ (b) $\eta_1 = +1$ and $\eta_2 = -1$

(c) $\eta_1 = -1$ and $\eta_2 = +1$ (d) $\eta_1 = -1$ and $\eta_2 = -1$

FIG. 4. (Color online) Nonzero components of the K matrix. Here, we consider two edges e and e', which belong to the same face f (otherwise $K_{e,e'} = 0$). Based on the local vertex-face correspondence, the face f is paired up with one of its vertices, which is marked by the (red) circle. We go around the face f from e to e' by following the direction of the positive orientation marked by the (blue) circle at the center of the face. In (a) and (b), the path from e to e' goes through the special site (marked by the red circle), and thus $\eta_1 = +1$. For (c) and (d), the special site is not on our path, and thus $\eta_1 = -1$. The sign of η_2 is determined by the orientation of e and e'. If their directions are both along (or opposite) to the direction of the positive orientation [(a) and (c)], $\eta_2 = +1$. Otherwise [(b) and (d)], $\eta_2 = -1$. Once η_1 and η_2 are determined, the value of $K_{e,e'}$ can be obtained as $K_{e,e'} = -\eta_1 \times \eta_2/2 = \pm 1/2$.

integral of A_e around f:

$$\Phi_f = \xi_{f,e} A_e. \tag{3.5}$$

Here, we sum over all edges and

$$\xi_{f,e} = \begin{cases} +1, & e \text{ is an edge of } f \text{ with positive orientation} \\ -1, & e \text{ is an edge of } f \text{ with negative orientation} \\ 0, & e \text{ is not an edge of } f. \end{cases} \tag{3.6}$$

The sign of $\xi_{f,e}$ is determined by going around the face f along the counterclockwise direction. If the direction of the edge e is along this path, $\xi_{f,e} = +1$. Otherwise, $\xi_{f,e} = -1$. As can be seen from Eq. (3.5), the matrix $\xi_{f,e}$ is a discretized curl operator $(\nabla\times)$ for planar graphs.

On a square lattice, the action that we constructed here reduces to the action found in Refs. [10,11], which can be considered as a special situation of our generic construction. Similarly, for the kagome lattice this general construction reduces to the construction that we presented in Ref. [12].

We conclude this section by comparing our discretized theory with the Chern-Simons gauge theory in the continuum. For comparison, we choose to write the action in the continuum in a special form

$$S = \frac{k}{2\pi} \int dt\, d\boldsymbol{x} \left(A_0 B - \frac{1}{2} A_i \epsilon_{i,j} \dot{A}_j \right). \tag{3.7}$$

Here, A_0 is the time component of the gauge field. A_i and A_j are the spatial components with i and j being x or y. $\epsilon_{i,j}$ is the Levi-Civita symbol and B is the magnetic field perpendicular to the 2D plane. The first term here enforces the flux attachment and the second term dictates the dynamics of the vector potentials A_x and A_y.

By comparing Eq. (3.4) with (3.7), we find that our discretized theory is in close analogy to the continuum case. Here, the M matrix dictates the flux attachment (i.e., Gauss' law) and the K matrix plays the role of the Levi-Civita symbol. It is worthwhile to highlight that, just as the Levi-Civita symbol, the K matrix is antisymmetric

$$K_{e,e'} = -K_{e',e}. \tag{3.8}$$

This can be verified easily by noticing that $\eta_1 \to -\eta_1$ and $\eta_2 \to \eta_2$, if we swap e and e'. This antisymmetry property is in fact expected. If we look at the second term in our action [Eq. (3.4)] because $\int dt\, A_e \dot{A}_{e'} = -\int dt\, \dot{A}_e A_{e'}$ (integration by part), only the antisymmetric part of K contributes to the action.

In the next six sections, we will demonstrate that our action indeed offers a discretized Chern-Simons gauge theory on generic graphs by showing that all the key properties of the Chern-Simons gauge theory are preserved by our action.

IV. GAUGE INVARIANCE

For a gauge theory, the action must be gauge invariant. In this section, we will verify that our action [Eq. (3.4)] preserves the gauge symmetry. In the case of Chern-Simons, this is also true provided the manifold has no boundaries. Furthermore, invariance under large gauge transformations (which wind around noncontractible loops of the systems) holds only if the index k is an integer [1]. These conditions are satisfied by our discretized Chern-Simons theory.

A. Gauge transformation on a graph

For a graph/lattice, a gauge transformation takes the following form:

$$A_v \to A_v - \partial_t \phi_v, \tag{4.1}$$

$$A_e \to A_e - D_{v,e} \phi_v, \tag{4.2}$$

where ϕ_v is an arbitrary scalar function defined on vertices. The first formula [Eq. (4.1)] is the gauge transformation for the time component of the gauge field, while the second one [Eq. (4.2)] is for the spatial components. The matrix $D_{v,e}$ in Eq. (4.2) is the *incident matrix* of the graph [48]

$$D_{v,e} = \begin{cases} +1 & \text{if } v \text{ is the positive end of } e, \\ -1 & \text{if } v \text{ is the negative end of } e, \\ 0 & \text{otherwise.} \end{cases} \tag{4.3}$$

Here, we called the vertex v a positive (negative) end of the edge e, if v is one of the two ends of e and the direction of the edge e is pointing towards (away from) v. The incident matrix contains all the information about the connectivity of the graph, as well as the direction assigned to each edge [48]. The incident matrix plays the role of a (discretized) gradient operator ∇, which can be seen easily by noticing that

$$D_{v,e}\phi_v = \phi_{v_1} - \phi_{v_2}, \tag{4.4}$$

where ϕ_v is an arbitrary scalar function and the edge e points from v_2 to v_1. As a result, Eq. (4.2) can be considered as a discretized version of $\boldsymbol{A} \to \boldsymbol{A} - \nabla\phi$. Later, we will show that the incident matrix also serves as a discretized divergence $\nabla\cdot$.

B. Gauge symmetry

As proven in Appendix C, the sufficient and necessary condition for the action of Eq. (3.4) to be gauge invariant is that the following identity is satisfied:

$$M_{v,f}\xi_{f,e} = K_{e,e'}D_{v,e'}, \tag{4.5}$$

where $\xi_{f,e}$ is defined in Eq. (3.6) and the incident matrix $D_{v,e'}$ is defined in Eq. (4.3). In this section, we prove that this condition is indeed valid for the M and K matrices constructed in Sec. III A.

To verify Eq. (4.5), we need to prove that the relation holds for any e and v. Here, we classify all possible situations into three cases:

(1) e and v do not belong to the same face.
(2) e and v belong to a same face, but v is not an end of e.
(3) v is an end of e.

Here, we verify Eq. (4.5) for each of these three cases.

1. Case I

The first case, where e and v do not belong to the same face, represents the situation where e and v are separated far away from each other. It is easy to verify that in this case, both sides of Eq. (4.5) vanish.

For the left-hand side, $M_{v,f} \neq 0$ requires v being a vertex of the face f and $\xi_{f,e} \neq 0$ requires e being an edge of f. For Case I, these two conditions cannot be satisfied simultaneously, and thus $M_{v,f}\xi_{f,e} = 0$.

For the right-hand side, $K_{e,e'} \neq 0$ implies that e and e' are edges of the same face, which will be called the face f. If $D_{v,e'} \neq 0$, v must be one end of e', which means that v is a vertex of f. As a result, to get a nonzero $K_{e,e'}D_{v,e'}$, both e and v must both belong to the same face f. This is in contradiction with the assumption of Case I, and thus we must have $K_{e,e'}D_{e',v} = 0$.

Because both sides of the equation are zero, then Eq. (4.5) holds for Case I.

2. Case II

The second case, where e and v belong to one same face but v is not an end of e, is shown in Fig. 5(a). In this figure, without loss of generality, we choose a specific direction for each edge. As proved in Appendix D, Eq. (4.5) is independent of the choice of the edge directions. Therefore, although we only consider one specific direction arrangement here, the conclusion is generic.

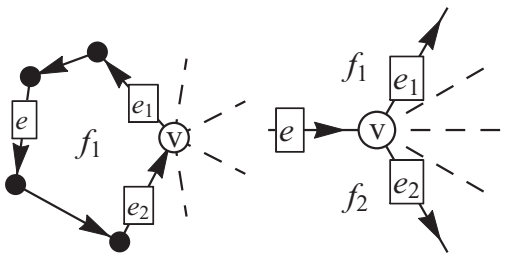

(a) Case II (b) Case III

FIG. 5. Gauge invariance of our theory for (a) Case II and (b) Case III. In (a), we marked two additional edges of v, e_1, and e_2, which are edges of f_1. In (b), we labeled two faces f_1 and f_2 and two additional edges e_1 and e_2, such that e is the common edge shared by f_1 and f_2, while e_1 and e_2 are two edges of v, which are adjacent to f_1 and f_2, respectively. Dashed lines represent (possible) additional edges of v, which are irrelevant for our proof and thus are not labeled. Although we assume a specific set of orientations for edges in these two figures, none of our final conclusions rely on the choice of orientations for each edge, as proven in Appendix C.

In Fig. 5(a), both v and e belong to the same face, f_1. Because v is a vertex of the face f_1, two of the edges of the face f_1 must have v as their end. These two edges are labeled as e_1 and e_2 in Fig. 5(a).

Using the edge directions shown in Fig. 5(a), it is easy to verify that

$$K_{e,e_1} = -\frac{\eta_{1;e,e_1}\eta_{2;e,e_1}}{2} = -\frac{\eta_{1;e,e_1}}{2}, \tag{4.6}$$

$$K_{e,e_2} = -\frac{\eta_{1;e,e_2}\eta_{2;e,e_2}}{2} = -\frac{\eta_{1;e,e_2}}{2}, \tag{4.7}$$

$$D_{v,e_1} = -1, \tag{4.8}$$

$$D_{v,e_2} = +1, \tag{4.9}$$

and thus

$$K_{e,e'}D_{v,e'} = K_{e,e_1}D_{v,e_1} + K_{e,e_2}D_{v,e_2} = \frac{\eta_{1;e,e_1} - \eta_{1;e,e_2}}{2}. \tag{4.10}$$

Here, we shall distinguish two different situations: (1) v is paired up with f_1 according to the vertex-face correspondence, and (2) v is not paired up with f_1.

If v is paired up with f_1, $M_{v,f}$ vanishes for all f, except for $f = f_1$, and, therefore,

$$M_{v,f}\xi_{f,e} = M_{v,f_1}\xi_{f_1,e} = +1. \tag{4.11}$$

Here, we do not sum over the repeated index f_1 and we used the fact that $M_{v,f_1} = 1$. For the orientation shown in Fig. 5(a), $\xi_{f_1,e} = +1$. For the right-hand side of Eq. (4.5), we can use Eq. (4.10). Here, we have $\eta_{1;e,e_1} = +1$ and $\eta_{1;e,e_2} = -1$ and, thus,

$$K_{e,e'}D_{e',v} = \frac{\eta_{1;e,e_1} - \eta_{1;e,e_2}}{2} = \frac{1}{2} + \frac{1}{2} = +1. \tag{4.12}$$

By comparing the two equations above, we find that $M_{v,f}\xi_{f,e} = K_{e,e'}D_{e',v}$

If v is not paired up with f_1, $M_{v,f_1}\xi_{f_1,e}=0$. For the right-hand side of Eq. (4.5), it is easy to verify that $\eta_{1;e,e_1}=\eta_{1;e,e_2}$, and thus

$$K_{e,e'}D_{e',v}=\frac{\eta_{1;e,e_1}-\eta_{1;e,e_2}}{2}=0. \tag{4.13}$$

Again, we verified Eq. (4.5).

3. Case III

For the last case, shown in Fig. 5(b), because each edge in our graph is shared by two and only two faces (as shown above in Sec. II), we can label the two faces of the edge e as f_1 and f_2. In addition, we also label two edges of v, e_1, and e_2, where e_1 is an edge of f_1 and e_2 is an edge of f_2. Because we have assumed that the graph and the dual graph are both *simple* (see Sec. II), $e_1\neq e_2$.

Same as in Case II, here too we only need to consider one specific set of directions for the edges and the conclusion will be generic. Using the directions shown in Fig. 5(b), we have

$$K_{e,e_1}=-\frac{\eta_{1;e,e_1}\eta_{2;e,e_1}}{2}=-\frac{\eta_{1;e,e_1}}{2}, \tag{4.14}$$

$$K_{e,e_2}=-\frac{\eta_{1;e,e_2}\eta_{2;e,e_2}}{2}=-\frac{\eta_{1;e,e_2}}{2}, \tag{4.15}$$

$$D_{v,e_1}=-1, \tag{4.16}$$

$$D_{v,e_2}=-1, \tag{4.17}$$

and therefore

$$\begin{aligned}K_{e,e'}D_{v,e'}=&K_{e,e_1}D_{v,e_1}+K_{e,e_2}D_{v,e_2}\\=&\frac{\eta_{1;e,e_1}+\eta_{1;e,e_2}}{2}.\end{aligned} \tag{4.18}$$

Again, we distinguish two possible situations: (1) v is paired up with f_1 or f_2 according to the vertex-face correspondence. (2) v is not paired up with either f_1 or f_2.

For the first situation, without loss of generality we assume that v is paired up with f_1. Using the directions shown in Fig. 5(b), we find that

$$M_{v,f}\xi_{f,e}=M_{v,f_1}\xi_{f_1,e}=+1. \tag{4.19}$$

Here, we do not sum over the repeated index f_1. In addition, we also have $\eta_{1;e,e_1}=\eta_{1;e,e_2}=+1$ and, therefore,

$$K_{e,e'}D_{e',v}=\frac{\eta_{1;e,e_1}+\eta_{1;e,e_2}}{2}=+1. \tag{4.20}$$

So, we find $M_{v,f}\xi_{f,e}=K_{e,e'}D_{e',v}$.

If v is not paired up with either f_1 or f_2, $M_{v,f}\xi_{f,e}=0$ because it is impossible to make both $M_{v,f}$ and $\xi_{f,e}$ nonzero. It is also easy to verify that here $\eta_{1;e,e_1}=-\eta_{1;e,e_1}$ and, thus,

$$K_{e,e'}D_{e',v}=\frac{\eta_{1;e,e_1}+\eta_{1;e,e_2}}{2}=0. \tag{4.21}$$

Once again, we get $M_{v,f}\xi_{f,e}=K_{e,e'}D_{e',v}$.

By summarizing all possible situations discussed above, we have verified Eq. (4.5). Therefore, we conclude that our theory is invariant under local gauge transformations.

V. FLUX ATTACHMENT

A key property of the Chern-Simons gauge theory is the constraint of flux attachment, which binds a magnetic flux with each charged particle. For a point charge q at location $\boldsymbol{r}_0$, the corresponding magnetic field is

$$B(\boldsymbol{r})=\frac{2\pi}{k}q\ \delta^2(\boldsymbol{r}-\boldsymbol{r}_0). \tag{5.1}$$

In the continuum classical theory, the flux and the charge are located at the same position, as indicated by the δ function in Eq. (5.1). In a continuum quantum gauge theory this condition is a constraint on the physical Hilbert space, and is the requirement that the quantum states be invariant under local time-independent gauge transformations [45], as we discussed in the Introduction [cf. Eq. (1.3)]. This condition requires regularization (in the form of splitting the position of the charge and the flux) which leads to a proper framing of the knots represented by Wilson loops [1,49,50]. For a discrete system, however, because electric charges live on vertices, while magnetic fluxes are defined on faces (which takes care of the regularization), it is necessary to specify one additional rule to dictate the location of the magnetic flux for charged particles at each site. This is achieved by the local vertex-face correspondence introduced in Sec. I. Here too, this constraint amounts to the conditions that the states of the gauge theory be invariant under time-independent gauge transformations [40].

Because our action [Eq. (3.4)] does not contain any dynamics for the time component of the gauge field A_v (just as in any gauge theory), A_v is not a dynamical field but its role is to enforce a constraint [45]. By taking a variational derivative of A_v, we get the charge at the vertex v,

$$q_v=\frac{\delta S}{\delta A_v}=\frac{k}{2\pi}M_{v,f}\Phi_f, \tag{5.2}$$

which is proportional to the magnetic flux in the face f. Because M is an orthogonal matrix, this equation implies that

$$\Phi_f=\frac{2\pi}{k}q_vM_{v,f}. \tag{5.3}$$

This equation is the discrete version of the flux attachment, analogous to Eq. (5.1).

Here, we find that for a charge at a vertex v, a magnetic flux is bound to it and the flux is located at the face f, which is the partner of v according to the vertex-face correspondence. This is the physical content of the vertex-face correspondence.

We conclude this section by emphasizing that the flux attachment rule here is *local* because we have required the vertex-face correspondence to be *local*, i.e., the magnetic flux attached to a charge is located on a neighboring face. For a discrete system, this setup offers the closest analogy to the delta function in Eq. (5.1).

VI. DUAL GRAPH, DUAL THEORY, AND THE INVERTIBILITY OF THE K MATRIX

In this section, we verify two key (and essential) properties of the discretized Chern-Simons gauge theory:

(1) The K matrix is invertible.

(2) For any discretized Chern-Simons gauge theory constructed above, one can construct another discretized Chern-Simons gauge theory on the dual graph.

Later, we will prove in Appendix E that the theory defined on the dual graph is in fact the dual theory of the original discretized Chern-Simons gauge theory.

As has been addressed in literature, the K matrix must be nonsingular (invertible) in order to ensure the correct dynamics for a discretized Chern-Simons gauge theory [10,11]. One way to realize this is by noticing that the inverse of the K matrix offers the commutator of the vector potential A_e (see Sec. VII for more details), and therefore, to avoid singularities in the commutator, the K matrix must be invertible.

Here, we will first verify the second property listed above by directly constructing a Chern-Simons gauge theory on the dual graph in Secs. VI A and VI B. Then, in Sec. VI C, we prove that K is invertible by finding directly the inverse matrix of K, which is in fact the K^* matrix defined on the dual graph with a minus sign. Finally, in Sec. VI D, as a consistency check, we prove that the gauge invariance condition for the original graph and that of the dual graph are actually equivalent to each other.

A. Duality transformation

For a planar graph G, one can construct the dual graph G^* by putting a vertex v^* in each face of G and then connecting two vertices in G^* if their corresponding faces in G share a common edge. It is easy to check that the dual of a dual graph is the original graph $(G^*)^* = G$. For the lattices shown in Fig. 2, the square lattice is self-dual, while the kagome lattice and the dice lattice are dual to each other.

For simplicity, we will use the same integer to label f and v^*, if f is mapped to v^* under the duality transformation. Similarly, we use the same integer to label e and e^* (v and f^*), if they are dual to each other. In addition, we choose the direction for each edge in the dual graph such that $\boldsymbol{n}_e \times \boldsymbol{n}_e^* > 0$, where $\boldsymbol{n}_e$ and $\boldsymbol{n}_e^*$ are unit vectors along the direction of the edge e and its dual edge e^*. In other words, we rotate the edge e counterclockwise until it aligns with e^*, and then the direction of the rotated edge e determines the direction of e^*.

With this convention, the incident matrix of the dual graph $D^*_{v^*,e^*}$ coincides with the $\xi_{f,e}$ matrix of the original graph [Eq. (3.6)]:

$$D^*_{v^*,e^*} = \xi_{f,e}. \tag{6.1}$$

Similarly, the $\xi^*_{f^*,e^*}$ matrix for the dual graph is in fact the incident matrix of the original graph D, up to an overall minus sign

$$\xi^*_{f^*,e^*} = -D_{v,e}. \tag{6.2}$$

Here, we require $v^* = f$ and $e^* = e$ as shown in the previous paragraph. The physics meaning of these two relations is that if the duality transformation maps a face f of a graph G into the vertex v^* in the dual graph G^*, then a loop around the face f is mapped to all the edges connected to vertex v^*, and vice versa.

It is easy to realize that under a duality transformation, the local vertex-face correspondence in the original graph is transformed into a local vertex-face correspondence in the dual graph. As a result, we can use exactly the same construction to obtain a discretized Chern-Simons gauge theory on the dual graph

$$S = \frac{k^*}{2\pi}\int dt\left[A^*_{v^*}M^*_{v^*,f^*}\Phi^*_{f^*} - \frac{1}{2}A^*_{e^*}K^*_{e^*,e'^*}\dot{A}^*_{e'^*}\right]. \tag{6.3}$$

Here, $A^*_{v^*}$ and $A^*_{e^*}$ are gauge fields defined on the dual graph with $\Phi^*_f = \xi^*_{f^*,e^*}A^*_e$ being the magnetic flux of this gauge field on face f^*. The M^* and K^* matrices are constructed using the same rules discussed above in Sec. III A. In Appendix E, we show that if $k^* = -1/k$, this action is the dual theory of the original discretized Chern-Simons gauge theory [Eq. (3.4)].

It is straightforward to verify that the M^* matrix is the transpose of the M matrix. Because M is an orthogonal matrix, it implies that M^* is the inverse of M

$$M^* = M^T = M^{-1}. \tag{6.4}$$

Following, we will study the K^* matrix and prove that it is the inverse of the K matrix up to an overall minus sign.

B. K^* matrix

In this section, we show that the K^* matrix can be constructed directly in the original graph G, without going to the dual graph G^*. This construction is fully equivalent to the dual-graph construction used in the previous section. However, as will be shown in the next section, by constructing the K^* matrix in the original graph, it is more convenient to study the relation between the K matrix and the K^* matrix.

As mentioned above, we label each edge in the dual graph using the same index as the corresponding edge in the original graph (i.e., $e^* = e$). Therefore, we can rewrite the K^* matrix using the edge indices of the original graph (e and e')

$$K^*_{e^*,e'^*} = K^*_{e,e'}, \tag{6.5}$$

where e and e' are edges of original lattice and they are dual to e^* and e'^*, respectively. The matrix $K^*_{e,e'}$ is now defined on the original graph, and thus we can translate the definition of the K^* matrix to the original graph. Using the original graph, it is straightforward to verify that

$$K^*_{e,e'} = \begin{cases} \pm\frac{1}{2} & \text{if } e \text{ and } e' \text{ share a vertex,} \\ 0 & \text{otherwise.} \end{cases} \tag{6.6}$$

If e and e' do not share a common end point, $K_{e,e'} = 0$. Otherwise,

$$K^*_{e,e'} = -\frac{\eta^*_1 \times \eta^*_2}{2} = \pm\frac{1}{2}, \tag{6.7}$$

where $\eta^*_1 = \pm 1$ and $\eta^*_2 = \pm 1$ are two Z_2 integers. To determine the sign of η^*_1, we first label the common end of e and e' as v. Under the vertex-face correspondence (of the original graph), v is paired up with a neighboring face f. Now, we go from the edge e to the edge e' by moving around v in the counterclockwise direction. If the path goes through the face f, $\eta^*_1 = +1$, and otherwise $\eta^*_1 = -1$. The sign of η^*_2 is determined by the directions of edges e and e'. If both of them point toward (or away from) v, $\eta^*_2 = +1$, and otherwise $\eta^*_2 = -1$.

C. $K^* = -K^{-1}$

In this section, we prove that

$$K^* = -K^{-1} \tag{6.8}$$

and thus K is invertible. To prove Eq. (6.8), we shall verify the following relations:

$$K_{e,e''}K^*_{e'',e'} = K^*_{e,e''}K_{e'',e'} = -\delta_{e,e'}, \tag{6.9}$$

where $\delta_{e,e'}$ is the Kronecker delta. In this section, we will only demonstrate $K_{e,e''}K^*_{e'',e'} = -\delta_{e,e'}$, while one can use the same method to prove $K^*_{e,e''}K_{e'',e'} = -\delta_{e,e'}$.

Here, we need to consider six different cases:

(1) $e = e'$.

(2) $e \neq e'$, and e and e' share an end point, and e and e' are edges of the same face.

(3) $e \neq e'$, and e and e' share an end point, but e and e' are not edges of the same face.

(4) e and e' do not share any end point, but belong to the same face.

(5) e and e' do not belong to the same face, but there is a face f, where e is an edge of f and one of the end points of e' is a vertex of f.

(6) Otherwise.

Among all the six cases, $\delta_{e,e'} = 1$ for the first one, and $\delta_{e,e'} = 0$ for all others. In Fig. 6, we show the first five cases. Here, we mark e, e' and all other edges that contribute to $K_{e,e''}K^*_{e'',e'}$ using solid lines. Other (possible) edges, which do not contribute to $K_{e,e''}K^*_{e'',e'}$, are labeled as dashed lines. Using

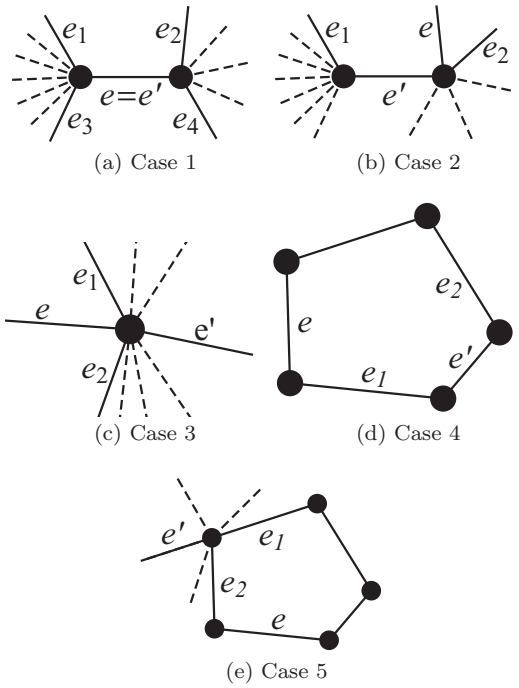

FIG. 6. Possible cases for computing $K_{e,e''}K^*_{e'',e'}$. Solid lines mark the edges e, e' and all edges that will contribute to $K_{e,e''}K^*_{e'',e'}$. Dashed lines are (possible) additional edges, which do not contribute to $K_{e,e''}K^*_{e'',e'}$.

Fig. 6, it is easy to notice that for all the first five situations

$$\begin{aligned} K_{e,e''}K^*_{e'',e'} &= \sum_i K_{e,e_i}K^*_{e_i,e'} \\ &= \sum_i \eta_{1;e,e_i}\eta_{2;e,e_i}\eta^*_{1;e_i,e'}\eta^*_{2;e_i,e'}. \end{aligned} \tag{6.10}$$

Here, for each e_i, η_1, η_2, η_1^*, and η_2^* are obtained using the rules defined above. Following, we compute $K_{e,e''}K^*_{e'',e'}$ for each situation using this formula.

1. Case 1

For the first situation [$e = e'$ as shown in Fig. 6(a)], we have

$$K_{e,e''}K^*_{e'',e'=e} = \sum_{i=1}^{4} K_{e,e_i}K^*_{e_i,e}. \tag{6.11}$$

Here, we do not sum over repeated indices on the right-hand side of the equation, and the four edges e_1, e_2, e_3, and e_4 are marked in Fig. 6(a). For any e_i, we can verify that $\eta_1 = \eta_1^*$ and $\eta_2 = -\eta_2^*$. Therefore, $K_{e,e_i} = -K^*_{e_i,e}$. As a result,

$$K_{e,e''}K^*_{e'',e'=e} = -\sum_{i=1}^{4}(K_{e,e_i})^2 = -\sum_{i=1}^{4}\left(\pm\frac{1}{2}\right)^2 = -1 \tag{6.12}$$

and, thus, we find that $K_{e,e''}K^*_{e'',e'} = -\delta_{e,e'}$ for $e = e'$.

2. Case 2

For the second case, shown in Fig. 6(b), it is straightforward to verify that if $\eta_{2;e,e_1}$ and $\eta_{2;e,e_2}$ have the same sign, then e_1 and e_2 must both point towards (or away from) the two vertices shown in Fig. 6(b). As a result, $\eta^*_{2;e_1,e'}$ and $\eta^*_{2;e_2,e'}$ must have opposite sign, and thus

$$\eta_{2;e,e_1}\eta^*_{2;e_1,e'} = -\eta_{2;e,e_2}\eta^*_{2;e_2,e'}. \tag{6.13}$$

Similarly, we can show that if $\eta_{2;e,e_1} = -\eta_{2;e,e_2}$, we must have $\eta^*_{2;e_1,e'} = \eta^*_{2;e_2,e'}$. And, therefore, Eq. (6.13) is always valid for Case 2.

For η_1's, we need to examine three different cases. Here, we consider the face f formed by e, e', e_1 and (possibly) other edges, and ask whether the vertex-face correspondence pairs up f with one of these two vertices. In general, there are three possibilities

(1) f is paired up with the vertex on the left.

(2) f is paired up with the vertex on the right.

(3) f is not paired up with either of them.

For the first situation, we have $\eta_{1;e,e_1} = -1$, $\eta^*_{1;e_1,e'} = -1$, and $\eta_{1;e,e_2} = \eta^*_{1;e_2,e'}$. Therefore, we find

$$\eta_{1;e,e_1}\eta^*_{1;e_1,e'} = \eta_{1;e,e_2}\eta^*_{1;e_2,e'}. \tag{6.14}$$

For the second situation, we have $\eta_{1;e,e_1} = -1$, $\eta^*_{1;e_1,e'} = +1$, and $\eta_{1;e,e_2} = -\eta^*_{1;e_2,e'}$. Therefore, Eq. (6.14) is still valid. For the third situation, it can be shown that $\eta_{1;e,e_1} = +1$, $\eta^*_{1;e_1,e'} = +1$, and $\eta_{1;e,e_2} = \eta^*_{1;e_2,e'}$. Thus, Eq. (6.14) is still valid.

In summary, we find that Eqs. (6.13) and (6.14) always hold for this case [Fig. 6(b)]. By multiplying these two equations

together, we get

$$K_{e,e_1}K^*_{e_1,e'} = -K_{e,e_2}K^*_{e_2,e'}. \tag{6.15}$$

Utilizing Eq. (6.10), this relation implies that $K_{e,e''}K^*_{e'',e'} = 0$, in agreement with the relation $K_{e,e''}K^*_{e'',e'} = -\delta_{e,e'}$.

3. Cases 3, 4, and 5

Using the same approach, we can show that for the third and the fourth cases, shown in Figs. 6(c) and 6(d),

$$\eta_{2;e,e_1}\eta^*_{2;e_1,e'} = \eta_{2;e,e_2}\eta^*_{2;e_2,e'}, \tag{6.16}$$

$$\eta_{1;e,e_1}\eta^*_{1;e_1,e'} = -\eta_{1;e,e_2}\eta^*_{1;e_2,e'}. \tag{6.17}$$

Once again, we get $K_{e,e''}K^*_{e'',e'} = 0 = -\delta_{e,e'}$.

For the fifth case, shown in Fig. 6(e), we have

$$\eta_{2;e,e_1}\eta^*_{2;e_1,e'} = -\eta_{2;e,e_2}\eta^*_{2;e_2,e'}, \tag{6.18}$$

$$\eta_{1;e,e_1}\eta^*_{1;e_1,e'} = \eta_{1;e,e_2}\eta^*_{1;e_2,e'}. \tag{6.19}$$

Thus, $K_{e,e''}K^*_{e'',e'} = 0 = -\delta_{e,e'}$.

4. Case 6

The last case, 6, is easy to verify because here e and e' are far away from each other, so that for any e'', either $K_{e,e''}$ or $K^*_{e'',e'}$ is zero. Therefore, $K_{e,e''}K^*_{e'',e'} = 0 = -\delta_{e,e'}$.

By summarizing all the possible cases, we conclude that $KK^* = -I$. We can use the same method to prove that $K^*K = -I$ and thus $K^* = -K^{-1}$. This result also proves that the K and K^* matrices that we constructed above are invertible.

D. Gauge invariance in the dual graph

As shown above in Sec. IV, in the original graph, our action of Eq. (3.4) is gauge invariant if and only if

$$M_{v,f}\xi_{f,e} = K_{e,e'}D_{v,e'}. \tag{6.20}$$

For the dual graph, there is a similar condition for the gauge invariance

$$M^*_{v^*,f^*}\xi^*_{f^*,e^*} = K^*_{e^*,e'^*}D^*_{v^*,e'^*}. \tag{6.21}$$

In this section, we prove that these two conditions are in fact equivalent as long as $M^* = M^{-1}$ and $K^* = -K^{-1}$.

We start from Eq. (6.21) and change the dual graph (face, edge, or vertex) labels into the corresponding labels of the original graph

$$M^*_{f,v}D_{v,e} = -K^*_{e,e'}\xi_{f,e'}, \tag{6.22}$$

and here we also use the relations $D^*_{v^*,e^*} = \xi_{f,e}$ and $\xi^*_{f^*,e^*} = -D_{v,e}$ [Eqs. (6.1) and (6.2)].

If $M^* = M^{-1}$ and $K^* = -K^{-1}$, the formula above implies that

$$M^{-1}_{f,v}D_{v,e} = K^{-1}_{e,e'}\xi_{f,e'}. \tag{6.23}$$

By multiplying the matrices M and K on both sides, we recover the condition of gauge invariance in the original graph, Eq. (4.5). Therefore, we find that the two gauge-invariance conditions (6.20) and (6.21) are equivalent.

VII. COMMUTATION RELATIONS AND THE K^{-1} MATRIX

The Chern-Simons theory in the continuum has a very special commutation relation. In particular, the commutator between the loop integrals of the vector potential is topologically invariant. We will show in this section that our discretized theory has the same property.

A. Commutators for the continuum case

For the Chern-Simons gauge theory in the continuum, for two arbitrary curves C and C', we have the following commutation relation:

$$\left[\int_C A, \int_{C'} A\right] = \frac{2\pi i}{k}\nu[C,C'], \tag{7.1}$$

where $\nu[C,C']$ is the number of (oriented) intersections between the two curves, i.e., the number of right-handed interactions of C and C' minus the number of left-handed ones [10].

If C and C' are closed loops, $\nu[C,C']$ is topologically invariant, and it is easy to verify that its value cannot change under any adiabatic procedures. In addition, if either C or C' can be contracted into a point (i.e., contractible), $\nu[C,C'] = 0$.

B. Canonical quantization

Using canonical quantization, it is straightforward to show that the conjugate field of the vector potential field A_{e_i} is

$$\frac{\delta S}{\delta \dot{A}_e} = \frac{k}{2\pi}K_{e,e'}A_{e'}. \tag{7.2}$$

This formula implies that for our discretized Chern-Simons theory, the vector potential A_e (and linear superpositions of A_e's) play both the role of the canonical coordinates and that of the canonical momenta. Because canonical coordinates and canonical momenta arise in pairs, this result requires that we must have even number of linear independent A_e's, i.e., the number of edges must be even. This is indeed true for any graphs considered here. Utilizing the Euler characteristic, we know that the numbers of vertices, edges, and faces must satisfy the following relation:

$$N_v - N_e + N_f = 2 - 2g, \tag{7.3}$$

where g is the genus of the underlying manifold. Because the vertex-face correspondence requires $N_v = N_f$, the number of edges is

$$N_e = 2N_f - 2 + 2g, \tag{7.4}$$

which is an even number.

In canonical quantization, the commutator between a canonical coordinate and the corresponding canonical momentum is $i\hbar$. Therefore, for our theory, we have

$$\left[A_e, \frac{k}{2\pi}K_{e',e''}A_{e''}\right] = i\delta_{e,e'}, \tag{7.5}$$

where $\delta_{e,e'}$ is the Kronecker delta and we set $\hbar$ to unity. Multiplying both sides by the inverse matrix of K, we obtain the commutation relation for the vector potential

$$[A_e, A_{e'}] = i\frac{2\pi}{k}K^{-1}_{e',e} = -\frac{2\pi i}{k}K^{-1}_{e,e'}. \tag{7.6}$$

Here, we used the fact that K^{-1} is an antisymmetric matrix.

In order to ensure that the commutator $[A_e, A_{e'}]$ is nonsingular, we must require the K matrix being invertible.

C. Paths, contractible and noncontractible cycles

In this section, we will introduce two concepts from the graph theory: *paths and cycles*, which are discrete versions of curves and loops, respectively [47].

A *path* is a sequence of vertices $v_0 \to v_1 \to v_2 \to \ldots \to v_m$, in which any two consecutive vertices are connected by an edge. In the literature of graph theory, it is often also assumed that a path never go through the same vertex twice. The length of a path is the total number of edges contained in the path.

If $v_0 \neq v_m$, the path is called *open*. For $v_0 = v_m$, the path is *closed*. A closed path (with nonzero length) is also called a *cycle*. In comparison with the continuum, it is easy to realize that open paths are discretized open curves, while cycles (i.e., closed paths) are discretized loops (i.e., closed curves). More precisely, a path (cycle) corresponds to a directed curve (loop) because a path (cycle) has a natural direction built in according to its definition, i.e., $v_0 \to \ldots \to v_m$.

In the continuum, loops on a 2D manifold can be classified into two categories: contractible or noncontractible, depending on whether or not the closed curve can be adiabatically contracted to a point. For a graph, there is a similar classification for cycles (closed paths) using a different but equivalent definition. We call a closed path (i.e., a cycle) contractible, if it is the boundary of some 2D area formed by a set of faces. Otherwise, it is noncontractible. For 2D closed and orientable surfaces in the continuum, noncontractible loops only exist for surfaces with nonzero genus (torus, double torus, etc.), while all loops on a genus zero surface (e.g., a sphere) are contractible. In graph theory, the same is true for cycles. For planar graphs defined on 2D closed and orientable surfaces, noncontractible cycles can only exist if the genus of the underlying 2D manifold is larger than zero.

For a directed graph (or lattice), each path (P) can be represented by an N_e-dimensional vector ξ_P, whose eth component is

$$\xi_{P,e} = \begin{cases} +1, & e \in P \text{ and } e \text{ is along the direction of } P \\ -1, & e \in P \text{ and } e \text{ is opposite to the direction of } P \\ 0, & e \notin P. \end{cases} \tag{7.7}$$

As will be shown in the following, this object defines a discretized line integral. In particular, if P is a cycle, $\xi_{P,e}$ provides a discretized loop integral.

D. Commutators and intersections

For a path P on a graph G, we can define the integral (circulation) of the vector potential along this path as

$$\mathcal{W}_P = \xi_{P,e} A_e. \tag{7.8}$$

This object is the discretized version of a line integral $\int_C \boldsymbol{A} \cdot d\boldsymbol{x}$ along a path C.

Now, we consider two different paths P and P', and we define two integrals $\mathcal{W}_P$ and $\mathcal{W}_{P'}$ for P and P', respectively, using the definition of Eq. (7.8). In this section, we prove that the commutator between $\mathcal{W}_P$ and $\mathcal{W}_{P'}$ is determined by the number of oriented intersections between the two paths $\nu[P, P']$:

$$[\mathcal{W}_P, \mathcal{W}_{P'}] = \frac{2\pi i}{k} \nu[P, P'], \tag{7.9}$$

which is the direct analog of the corresponding commutator of the Chern-Simons theory in the continuum (7.1).

Utilizing the commutator of Eq. (7.6), we find

$$[\mathcal{W}_P, \mathcal{W}_{P'}] = -\frac{2\pi i}{k} \xi_{P,e} \xi_{P',e'} K^{-1}_{e,e'}. \tag{7.10}$$

If the two paths P and P' share no common vertex, the intersection number is obviously zero $\nu[P, P'] = 0$. In the same time, $[\mathcal{W}_P, \mathcal{W}_{P'}]$ also vanishes because every term on the right-hand side of Eq. (7.10) is zero.

If the two paths share some common vertices, only edges connected to these common vertices contribute to the commutator of Eq. (7.10) because $K^{-1}_{e,e'} = 0$ for all other edges. Therefore, we only need to consider edges adjacent to each common vertex. As shown in Fig. 7, we shall distinguish three different situations, shown in Figs. 7(a)–7(c), respectively, depending on whether the common vertex is a right-handed intersection, a left-handed intersection, or not an intersection. In Fig. 7, we label the edges of P as e_1 and e_2, while the edges of P' are called e'_1 and e'_2. Using Eq. (7.10), the commutator

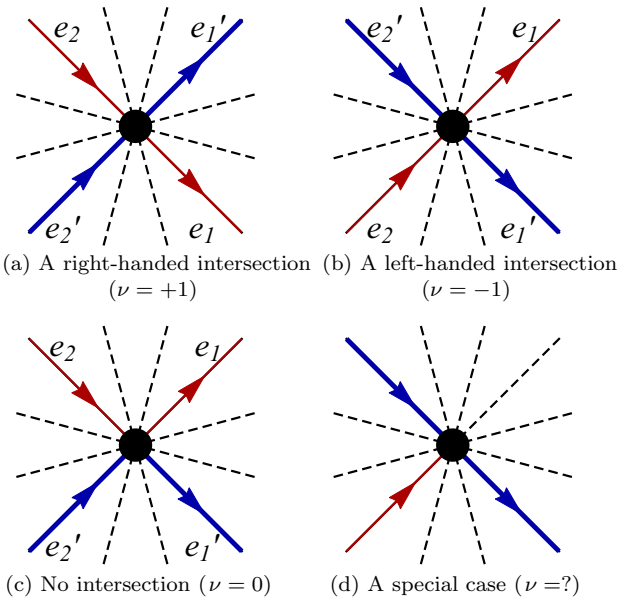

(a) A right-handed intersection ($\nu = +1$) (b) A left-handed intersection ($\nu = -1$)

(c) No intersection ($\nu = 0$) (d) A special case ($\nu = ?$)

FIG. 7. (Color online) One common vertex shared by two paths. Here, we consider two paths P (thin red solid lines) and P' (thick blue solid lines). The arrows indicate the direction of each path. The disk in the middle is one common vertex shared by the two paths. Dashed lines represent other (possible) edges that are connected to the vertex, and they do not contribte to the commutator that we want to compute. (a) shows a right-handed intersection between P and P' and (b) is a left-handed one. In (c), the two paths do not intersect. (d) Shows a special case, where one path terminates at this vertex. Here, the number of intersections can be ± 1 or 0 depending on microscopic details. In Sec. VII E, a method will be introduced to obtain the value of ν for (d) by defining a dual path in the dual graph.

is given by

$$[\mathcal{W}_P,\mathcal{W}_{P'}] = \frac{2\pi i}{k}\sum_{i=1}^{2}\sum_{j=1}^{2}\xi_{P,e_i}\xi_{P',e'_i}K^*_{e_i,e'_i} = -\frac{2\pi i}{k}\frac{1}{2}\sum_{i=1}^{2}\sum_{j=1}^{2}\xi_{P,e_i}\xi_{P',e'_j}\eta^*_{1;e_i,e'_j}\eta^*_{2;e_i,e'_j}. \tag{7.11}$$

Here, we used the fact that $K^{-1} = -K^*$ and each element of K^* can be written as $-\eta^*_1\eta^*_2/2$ as defined in Sec. VI. For the first three figures in Fig. 7, it is easy to verify that

$$\xi_{P,e_i}\xi_{P',e'_j}\eta^*_{2;e_i,e'_j} = \begin{cases} +1 & \text{if } i = j, \\ -1 & \text{if } i \neq j. \end{cases} \tag{7.12}$$

If the common vertex is a right-handed intersection of P and P' [Fig. 7(a)], four possible cases need to be considered depending on the location of the face that paired up with the common vertex, i.e., (1) between e'_1 and e_2, (2) between e_2 and e'_2, (3) between e'_2 and e_1, and (4) between e_1 and e'_1. For case (1), we have $\eta^*_{1;e_1,e'_1} = -1$, $\eta^*_{1;e_1,e'_2} = +1$, $\eta^*_{1;e_2,e'_1} = -1$, and $\eta^*_{1;e_2,e'_2} = -1$. For case (2), we have $\eta^*_{1;e_1,e'_1} = -1$, $\eta^*_{1;e_1,e'_2} = +1$, $\eta^*_{1;e_2,e'_1} = +1$, and $\eta^*_{1;e_2,e'_2} = +1$. For case (3), $\eta^*_{1;e_1,e'_1} = -1$, $\eta^*_{1;e_1,e'_2} = -1$, $\eta^*_{1;e_2,e'_1} = +1$, and $\eta^*_{1;e_2,e'_2} = -1$. For case (4), $\eta^*_{1;e_1,e'_1} = +1$, $\eta^*_{1;e_1,e'_2} = +1$, $\eta^*_{1;e_2,e'_1} = +1$, and $\eta^*_{1;e_2,e'_2} = -1$. Using Eqs. (7.11) and (7.12), we find that for all these four cases, the commutator $[\mathcal{W}_P,\mathcal{W}_{P'}] = 2\pi i/k$. Therefore, we find that each right-handed intersection contributes $2\pi i/k$ to the commutator.

Using the same technique, we can prove $[\mathcal{W}_P,\mathcal{W}_{P'}] = -2\pi i/k$ for Fig. 7(b), and $[\mathcal{W}_P,\mathcal{W}_{P'}] = 0$ for Fig. 7(c). In summary, we find that each right-handed (left-handed) intersection contributes $+2\pi i/k$ ($-2\pi i/k$) to the commutator $[\mathcal{W}_P,\mathcal{W}_{P'}]$, and thus we proved Eq. (7.9).

E. Gauge invariance and the commutation relations

In this section, we prove that the commutation relations of Eq. (7.9) arise naturally, if we require the action to be gauge invariant [Eq. (4.5)]. In addition, a by-product of this proof offers a more rigorous definition for the number of oriented intersections, which eliminates the ambiguity demonstrated in Fig. 7(d). There, the two paths P and P' barely touch each other. Shall this count as an intersection? This question will be answered in this section.

Consider two paths P and P'. Here, we assume that one of the paths is a contractible cycle (P'), while the other is an open path with two open ends (P). As an example, a contractible cycle P' is plotted in Fig. 8. Because P' is contractible, it is the edge of an area formed by a set of faces (the dark region in Fig. 8). Utilizing the vertex-face correspondence, this set of faces is mapped to a set of vertices, which is marked by circles in Fig. 8. Now, we can define a cycle in the dual lattice such that the cycle encloses (and only encloses) these vertices (the dashed lines in Fig. 8). This new cycle will be called the dual of P' and will be labeled as P'^*. Here, we choose the direction of P'^* such that its orientation is the same as that of P'. Following, we will prove that the gauge invariance

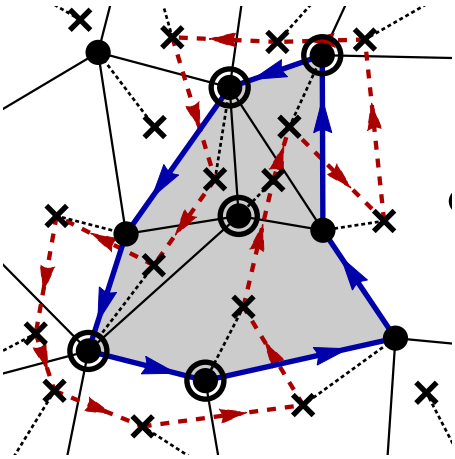

FIG. 8. (Color online) A cycle in a graph and the dual cycle in the dual graph. Here, we consider a planar graph with a local face-vertex correspondence. The vertices in the original graph are marked by disks, while the crosses label the faces, i.e., vertices of the dual graph. The local face-vertex correspondence is marked using the dotted lines, which pair up each face with one of its neighboring vertex. The thick solid (blue) lines marks a contractible cycle (a closed path) and the orientation of the cycle is marked by the arrows. For a contractible cycle, its interior is formed by a set of faces (dark region). For each face inside the dark region, we find the corresponding vertex using the local face-vertex correspondence. These vertices are marked by circles. Then, we draw a loop in the dual graph, which encloses these vertices (red dashed lines connecting neighboring crosses). This loop in the dual graph is the dual of the original loop in the original graph. And, we require the two loops to have the same orientation.

immediately implies the commutator

$$[\mathcal{W}_P,\mathcal{W}_{P'}] = \frac{2\pi i}{k}\nu[P,P'^*]. \tag{7.13}$$

Here, instead of the number of intersections between P and P', we shall count the number of intersections for P and P'^*. Because the cycle P'^* is defined in the dual graph, the number of intersections is always well-defined and this eliminates the ambiguity shown in Fig. 7(d).

Before proving Eq. (7.13), we would like to highlight that although the dual cycle P'^* and the original cycle P are not identical, the difference between them is local and microscopic. This comes from the fact that our vertex-face correspondence is *local*, where a face is paired with one of its neighboring vertex. If we take the continuous limit and ignore differences at the microscopic level, the differences between P'^* and P' vanish and, therefore, we recover Eq. (7.1).

Now, we prove Eq. (7.13). First, we define a N_f-dimensional vector $Q_{P'}$ for the contractible cycle P', whose fth component $Q_{P',f}$ is

$$Q_{P',f} = \begin{cases} 1 & \text{if the face } f \text{ is enclosed by } P', \\ 0 & \text{if the face } f \text{ is outside of } P'. \end{cases} \tag{7.14}$$

With this matrix $Q_{P',f}$, the contractible cycle P' can be written as

$$\xi_{P',e} = Q_{P',f}\xi_{f,e}, \tag{7.15}$$

where $\xi_{f,e}$ is defined in Eq. (3.6) and $\xi_{P,e}$ is defined in Eq. (7.7). The proof for Eq. (7.15) is straightforward. For the right-hand side, it is easy to notice that for any e outside the region enclosed by the cycle P', $Q_{P',f}\xi_{f,e}=0$. For an edge inside the region enclosed by the cycle P', it will induce two terms for the right-hand side because each edge is shared by two faces. These two terms have opposite signs and thus cancel out, and thus $Q_{P',f}\xi_{f,e}=0$. The only way to have a nonzero $Q_{P',f}\xi_{f,e}$ is to require that e is an edge of the cycle P'. And it can be verified that the value and the sign of $Q_{P',f}\xi_{f,e}$ match exactly $\xi_{P',e}$.

Similarly, in the dual space, we can write the dual cycle P'^* as

$$\xi^*_{P'^*,e^*}=Q^*_{P'^*,f^*}\xi^*_{f^*,e^*}=-Q^*_{P'^*,v}D_{v,e}, \tag{7.16}$$

where $Q^*_{P'^*,f^*}=1$ for any faces (of the dual graph) inside the dual cycle P'^*. Here, we relabeled the faces in the dual graph (f^*) using corresponding vertices in the original graph (v). We also used the fact that $\xi^*_{f^*,e^*}=-D_{v,e}$ as shown in Eq. (6.2). Because the vertices (of the original graph) enclosed by P'^* are partners of the faces enclosed by P', we have

$$Q^*_{P'^*,v}=Q_{P',f}M_{v,f}. \tag{7.17}$$

By combining the two equations above and relabeling e^* as e, we find that

$$\xi^*_{P'^*,e}=-Q_{P',f}M^{-1}_{f,v}D_{v,e}. \tag{7.18}$$

In the last step, we used the fact that the M matrix is orthogonal, $M_{v,f}=M^{-1}_{f,v}$.

By substituting Eq. (7.15) into (7.10), we find that

$$\begin{aligned}[\mathcal{W}_P,\mathcal{W}'_P]&=-\frac{2\pi i}{k}\xi_{P,e}K^{-1}_{e,e'}\xi_{P',e'}\\&=-\frac{2\pi i}{k}\xi_{P,e}K^{-1}_{e,e'}Q_{P',f}\xi_{f,e'}\\&=-\frac{2\pi i}{k}\xi_{P,e}Q_{P',f}M^{-1}_{f,v}D_{v,e}.\end{aligned} \tag{7.19}$$

Here, we utilized the condition of gauge invariance $M^{-1}_{f,v}D_{v,e}=K^{-1}_{e,e'}\xi_{f,e'}$ [Eq. (6.23)]. Using Eq. (7.18), the right-hand side can be written as

$$[\mathcal{W}_P,\mathcal{W}'_P]=\frac{2\pi i}{k}\xi_{P,e}\xi^*_{P'^*,e}. \tag{7.20}$$

It is easy to verify that only intersections between P and P'^* contribute to the right-hand side of the equation. At a right-handed/left-handed intersection, $\xi_{P,e}\xi^*_{P'^*,e}=\pm1$, and thus

$$[\mathcal{W}_P,\mathcal{W}'_P]=\frac{2\pi i}{k}\nu[P,P'^*]. \tag{7.21}$$

VIII. WILSON LOOPS FOR NONCONTRACTIBLE CYCLES

We start this section by considering a planar graph embedded on a 2D torus (with genus $g=1$). For this graph, there are two independent noncontractible cycles (i.e., discretized counterparts of the two noncontractible loops on a torus), which will be labeled as C and C' in this section. These two cycles intersect once with each other. Without loss of generality, we choose the oriented intersection number to be $+1$, instead of -1, i.e., $\nu[C,C']=+1$. As we proved above in Eq. (7.9), the commutator $[\mathcal{W}_C,\mathcal{W}_{C'}]=2\pi i/k$.

Here, we define Wilson loops for the two noncontractible cycles C and C' of the torus

$$W_C=\exp(i\mathcal{W}_C), \tag{8.1}$$

$$W_{C'}=\exp(i\mathcal{W}_{C'}). \tag{8.2}$$

Because the commutator $[\mathcal{W}_C,\mathcal{W}_{C'}]=2\pi i/k$ is a complex number (i.e., is proportional to the identity operator), it commutes with both $\mathcal{W}_C$ and $\mathcal{W}_{C'}$. Hence, using the Baker-Hausdorff-Campbell formula, it follows that

$$e^{i\mathcal{W}_C}e^{i\mathcal{W}_{C'}}=e^{i\mathcal{W}_{C'}}e^{i\mathcal{W}_C}e^{[i\mathcal{W}_C,i\mathcal{W}_{C'}]} \tag{8.3}$$

and thus

$$W_CW_{C'}=W_{C'}W_Ce^{-2\pi i/k}. \tag{8.4}$$

If we consider an eigenstate of W_C with eigenvalue w,

$$W_C|\Psi\rangle=w|\Psi\rangle, \tag{8.5}$$

where w is a complex number, utilizing Eq. (8.4), it is straightforward to show that $W_{C'}|\Psi\rangle$ is also an eigenstate of W_C and its eigenvalue is $we^{-2\pi i/k}$:

$$W_C(W_{C'}|\Psi\rangle)=we^{-2\pi i/k}(W_{C'}|\Psi\rangle). \tag{8.6}$$

In other words, we can consider $W_{C'}$ as a raising/lowering operator for the operator W_C, and vice versa. Starting from the eigenstate $|\Psi\rangle$, eigenstates of W_C can be generated by applying this raising/lowering operator

$$W_C\left(W^n_{C'}|\Psi\rangle\right)=we^{-2n\pi i/k}\left(W^n_{C'}|\Psi\rangle\right), \tag{8.7}$$

i.e., $W^n_{C'}|\Psi\rangle$ is an eigenstate with eigenvalue $we^{-2n\pi i/k}$.

For an integer k, it is easy to note that when $n=k$, the state $W^k_{C'}|\Psi\rangle$ has the same eigenvalues as $|\Psi\rangle$. If $W^k_{C'}|\Psi\rangle$ and $|\Psi\rangle$ are the same quantum state, $W^n_{P'}|\Psi\rangle$ generates k different eigenstates of W_P. From this result it follows that the well-known result that a Chern-Simons gauge theory has a k-fold topological degeneracy on a torus. This conclusion is well known in the continuum. Our discussion above shows that the same is true in our discretized theory.

It is straightforward to generate the discussion above to other 2D manifolds with different genus. For a planar graph defined on a 2D surface with genus g, there are $2g$ independent noncontractible cycles. As will be discussed in Sec. X (Fig. 9), we can choose g of these cycles such that they do not intersect

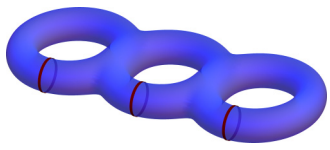

FIG. 9. (Color online) Noncontractible cycles on a surface with nonzero genus. For a genus g surface, we can choose g-independent noncontractible cycles, which do not intersect with one another. These g cycles will be used as vector ξ_i with $i=N_f,N_f+1,\ldots,N_f+g-1$, in our complete basis for the edge space. Here, we show an example with $g=3$. The three red loops mark three independent noncontractible cycles without any intersections.

with each other, $C_1, C_2, \ldots, C_g$. The other g noncontractible cycles will be labeled $C_1', C_2', \ldots, C_g'$. The absence of intersection for cycles C_i $(i = 1,2,\ldots,g)$ implies that the Wilson loops defined on this cycle commute with each other, and thus we can consider common eigenstates for $W_{C_1}, W_{C_2}, \ldots, W_{C_g}$. The Wilson loops for the other g noncontractible cycles serve as raising and lowering operators. Starting from one common eigenstate of all W_{C_i}'s, we can use $W_{C_i'}$ to generate k^g eigenstates (including the original one), which reflects the topological degeneracy of the Chern-Simons gauge theory on a surface with genus g.

IX. LOCALITY

In this section, we verify that our theory is *local*. More precisely, we prove that (1) our action is local, i.e., the action does not have any coupling between fields that are not around the same face, (2) the flux attachment is local, i.e., for a charge at the vertex v, its magnetic flux must be located on a neighboring face, and (3) the commutator between vector potentials is *local*, i.e., for any two edges that do share a common vertex, the vector fields defined on them commute with each other.

A. The action

In the discretized action of Eq. (3.4), there are no long-range couplings beyond edges and vertices of the same face. In the first term in Eq. (3.4), because $M_{f,v}$ vanishes unless f and v are adjacent to each other, the action only contains couplings between nearby A_v and A_e (i.e., e and v must belong to the same face). For the second term, we know that $K_{e,e'} = 0$, if e and e' do not belong to the same face, and therefore, only short-range coupling (for edges of the same face) is included in this term.

B. Flux attachment

For the Chern-Simons gauge theory in the continuum, the flux attachment is *local*, i.e., for a point charge at r_0, the magnetic field is a delta function $B \propto \delta(\vec{r} - \vec{r}_0)$, and the B field vanishes when we move away from the point charge.

In our discretized theory, this condition of locality is preserved to the maximum extent. As shown in Eq. (5.3), for a charge at the site v, the corresponding magnetic field only is present inside *a single face*, which is the closest analog of a delta function in a discrete setup. As for the relative locations of the charge and its flux, because these two objects are on different parts of the graph (charges on vertices and fluxes on faces), it is impossible to require their location to coincide. Instead, we require the charge and the flux to be adjacent to each other.

We emphasize that this locality condition plays a very important role, if we use the Chern-Simons gauge theory as a statistical field to change the statistics for matter fields coupled to it. To ensure that all particles have the correct statistics, when we move a particle A around another particle B, A must feel all the statistical field of B. In other words, no matter which path we choose, as long as A moves around B, the magnetic flux attached to B must be enclosed by the path of A. For our theory (and for the continuous Chern-Simons gauge theory), this is always true. However, if one were to violate the locality condition by putting the magnetic flux in a face not adjacent to the charge, it would be possible to move A around B without enclosing the flux inside the path. As a result, the statistics of the matter field would become ill defined.

C. Commutation relations

As shown in Eq. (7.6), the commutator for the vector potential is determined by the inverse of the K matrix (or say the dual matrix K^*). As proved in Sec. VI, the K^{-1} matrix is also local, where the matrix element $K^{-1}_{e,e'} = 0$, if e and e' do not share a common vertex.

This results imply that a nonzero commutator can only arise for two neighboring edges, while for two edges separated away from each other (i.e., not sharing a common vertex), the vector potential always commutes with each other.

X. WHY $N_v = N_f$?

Above, we have shown that the existence of a local vertex-face correspondence is sufficient for the discretization of the Chern-Simons gauge theory. In this section, we prove that this condition is also necessary, if we want to preserve key properties of the Chern-Simons theory.

Let us consider a generic discretized action of gauge fields A_v and A_e. Just as in the Chern-Simons gauge theory in the continuum, we assume that the action does not contain time derivatives of the time component of the gauge field A_v, and that A_v plays the role of a Lagrange multiplier field that enforces a constraint on the local flux. For the coupling among the components of the gauge fields A_e on different edges, the action only contains product between A_e and $\partial_t A_{e'}$. We ignore possible terms with higher orders in time derivatives, which are less relevant in the sense of the renormalization group. In addition, we will only keep terms to the leading order in our action.

With these assumptions, the most generic action that one can write is

$$S = \frac{k}{2\pi} \int dt \left[A_v M_{v,f} \xi_{f,e} A_e - \frac{1}{2} A_e K_{e,e'} \dot{A}_{e'} \right]. \qquad (10.1)$$

This action is very similar to the action we constructed above in Eq. (3.4). However, we must emphasize that here M and K are generic matrices, and that so far we are not putting any constraints on them. Most importantly, now we do not require the graph to support a local vertex-face correspondence. Instead, we will consider generic situation and show that if we want the action to take this form, then the local vertex-face correspondence will arise naturally.

In Sec. X A, we first introduce some mathematical tools from algebraic graph theory. Then, in Sec. X B, we will prove that the number of faces cannot exceed the number of vertices ($N_v \geqslant N_f$), and otherwise the theory will be singular. Then, in Sec. X C, we show that the flux attachment requires the number of vertices not to exceed the number of faces ($N_v \leqslant N_f$). Combining these two conclusions together, we find that the graph must have the same number of vertices and faces ($N_v = N_f$). Finally, in Sec. X D, we prove that a local vertex-flux correspondence is necessary, if we further require the flux attachment to be local.

A. Edge space, cut space, and loop space

Here, we introduce some concepts from the algebra graph theory [48], that will be used later. In algebraic graph theory, an N_e-dimensional vector represents each edge e of a graph G,

$$\epsilon_e = (0,0,\ldots,1,\ldots,0), \tag{10.2}$$

where the eth component of the vector is 1 and all other components are 0. These vectors form the basis of a N_e-dimensional linear space, which is called the *edge space* of the graph G. It is easy to realize that the K matrix defined above is a rank-2 tensor in this linear space.

For a directed graph (i.e., a digraph), each (contractible or noncontractible) cycle C can be represented as an N_e-dimensional vector ξ_C, whose eth component is

$$\xi_{C,e} = \begin{cases} +1, & e \in C \text{ and } e \text{ is along the direction of } C \\ -1, & e \in C \text{ and } e \text{ is opposite to the direction of } C \\ 0, & e \notin C. \end{cases} \tag{10.3}$$

These vectors span a linear space, which is a subspace of the edge space. In algebraic graph theory, this subspace is known as the *circuit subspace*.

A *cut set* is a set of edges, where if we cut all the edges in a cut set, the graph is cut into two disconnected pieces. A more rigorous definition of a cut set relies on a partition of vertices. If V is the set of all vertices of a graph G, we can separate these vertices into two subsets V_1 and V_2, such that $V_1 \cup V_2 = V$ and $V_1 \cap V_2 = 0$. This is called a partition of the set V. For each partition of V, we can define a cut set by collecting all edges of G that have one end in V_1 and the other in V_2. For a digraph, one can choose one of the two possible orientations for a cut set by specifying the vertices in V_1 (or V_2) to be the positive ends, while the other to be negative. If an edge in the cut set points to the positive end of the cut set, it is a positive edge in this cut set. Otherwise, it is a negative edge.

Similar to cycles discussed above, each cut set can also be represented by an N_e-dimensional vector ξ_H, whose eth component is

$$\xi_{H,e} = \begin{cases} +1, & e \in H \text{ and } e \text{ is a positive edge} \\ -1, & e \in H \text{ and } e \text{ is a negative edge} \\ 0, & e \notin H. \end{cases} \tag{10.4}$$

The linear space spanned by these vectors is known as the *cut subspace*, which is also a subspace of the edge space. For a planar graph, each cut set corresponds to a contractible cycle in the dual graph.

In algebraic graph theory, it is shown that the edge space is the direct sum of the circuit subspace and the cut subspace. In Appendix F, we provide a proof for the planar graphs considered here. This result implies that for the edge space, instead of using the basis shown above in Eq. (10.2), we can choose a new basis for the edge space by selecting a complete basis of the circuit subspace and a complete basis of the cut subspace.

For planar graphs, we can use all independent (contractible or noncontractible) cycles to form a basis for the circuit subspace. For the cut subspace, all independent contractible cycles in the dual graph form a complete basis. Therefore, we can span the edge space using these loops. Using this new basis, we can rewrite all tensors defined on the edge space, including the K^{-1} matrix, which will be done in the next section.

B. $N_v \geqslant N_f$

We will now prove that for the K matrix to be nonsingular and the discretized theory to preserve the correct commutation relation of Eq. (7.1), the number of faces can never exceed the number of vertices. Using the generic action shown in Eq. (10.1) (remember that K and M are now two arbitrary matrices), we find that for the generic setup, we shall still expect the commutation relation

$$[A_e, A_{e'}] = -\frac{2\pi i}{k} K^{-1}_{e,e'}. \tag{10.5}$$

Because singularities in the commutation relations must be avoided, the K matrix must be invertible. In addition, if we consider two cycles (loops) C and C', we shall expect the commutation relation

$$[\mathcal{W}_C, \mathcal{W}_{C'}] = \frac{2\pi i}{k} \nu[C,C']. \tag{10.6}$$

As shown above, this commutator is a topological invariant and it is one of the key features of the Chern-Simons gauge theory. Thus, we will require Eq. (10.6) for our discretized theory.

In the following, we prove that if we assume the topologically invariant commutation relation (10.6), then the K matrix must be singular if $N_v < N_f$. Therefore, we must have $N_v \geqslant N_f$. We will start from a genus zero surface and then expand the conclusion to other surfaces with nonzero genus.

1. *Graphs on a genus zero surface*

Here, we consider graphs defined on a genus zero surface (a sphere). Instead of directly showing that the K matrix is singular for $N_v < N_f$, here we take a different but equivalent approach. We will start by assuming the K matrix is invertible and work with the K^{-1} matrix. Then, using the commutation relation, we will show that the determinant of K^{-1} matrix is zero for $N_v < N_f$, and thus the K matrix is singular.

Using Eqs. (10.5) and (10.6), we know that

$$K^{-1}_{e,e'} \xi_{C,e} \xi_{C',e'} = -\nu[C,C']. \tag{10.7}$$

Here, we choose a new basis set for the edge space. Instead of using the vectors shown in Eq. (10.2), we use a set of vectors ξ_i with $i = 1,2,\ldots,N_e$. For $i = 1,2,\ldots,N_f - 1$, ξ_i are independent cycles, i.e., they form a complete basis of the circuit subspace. For $i = N_f, N_f + 1, \ldots, N_e$, the corresponding ξ_i are independent cut sets, i.e., they are a complete basis of the cut subspace. Using this new basis, we can define a $\tilde{K}^{-1}$ matrix as

$$\tilde{K}^{-1}_{i,j} = K^{-1}_{e,e'} \xi_{i,e} \xi_{j,e'}. \tag{10.8}$$

For i and j smaller than N_f, ξ_i and ξ_j are contractible cycles of the graph (for a planar defined on a closed orientable 2D surface with genus zero, all cycles are contractible). Using Eq. (10.7), it is easy to realize that $\tilde{K}^{-1}_{i,j} = 0$ for i and j smaller than N_f. (As shown above, the number of oriented

intersections for contractible loops is always zero). Therefore, we can write the $\tilde{K}^{-1}$ matrix in a block form

$$\tilde{K}^{-1} = \begin{pmatrix} 0 & A \\ -A^T & B \end{pmatrix}. \tag{10.9}$$

Here, the first block 0 is a $(N_f - 1) \times (N_f - 1)$ zero matrix and B is a $(N_e - N_f + 1) \times (N_e - N_f + 1)$ matrix. Using the Euler characteristic $N_v - N_e + N_f = 2 - 2g$, we can rewrite the dimensions of B as $(N_v - 1) \times (N_v - 1)$ since we have assumed the genus being zero, $g = 0$. The block A has dimension $(N_f - 1) \times (N_v - 1)$ and A^T is the transpose of A.

For a matrix with a block of zeros as shown in Eq. (10.9), the determinant of the matrix must be zero, if the zero block is larger than the B block (see Appendix G for a proof). Therefore, if $N_v < N_f$, $\det \tilde{K}^{-1} = 0$. Because ξ_i is a complete basis for the edge space, this implies that $\det K^{-1} = 0$ and thus K is a singular matrix.

2. *Surfaces with nonzero genus*

For a surface with nonzero genus, the same conclusion can be proved. Here, we choose the following basis of the edge space $\xi_1, \xi_2, \ldots, \xi_{N_e}$. For $i = 1, 2, \ldots, N_f - 1$, ξ_i are $N_f - 1$ independent contractible cycles. Then, for $i = N_f, N_f + 1, \ldots, N_f + 2g - 1$, ξ_i are independent noncontractible cycles. For these noncontractible cycles, we choose to have the first g noncontractible cycles ($N_f \leqslant i \leqslant N_f + g - 1$) not to cross with one another as shown in Fig. 9. It is easy to realize that the first $N_f + 2g - 1$ vectors here form a basis of the circuit subspace, while the rest are chosen to be a complete basis of the cut subspace.

Using this new basis, we can define a $\tilde{K}^{-1}$ matrix as

$$\tilde{K}^{-1}_{i,j} = K^{-1}_{e,e'} \xi_{i,e} \xi_{j,e'}. \tag{10.10}$$

For $i < N_f$ and $j < N_f + g$ (or $i < N_f + g$ and $i < N_f$), $\tilde{K}^{-1}_{i,j} = 0$. This is because here ξ_i and ξ_j are to cycles of the graph G and at least one of them is contractible. According to Eq. (10.7), $\tilde{K}^{-1}_{i,j} = 0$ because the number of oriented intersections vanish when one of the cycles is contractible. For $N_f \leqslant i \leqslant N_f + g - 1$ and $N_f \leqslant j \leqslant N_f + g - 1$, ξ_i and ξ_j are two noncontractible cycles, but we have required that these cycles do not cross each other, i.e., $\nu[\xi_i, \xi_j] = 0$, and thus, $\tilde{K}^{-1}_{i,j} = 0$.

With this knowledge, we can write the matrix $\tilde{K}_{i,j}$ in this block form

$$\tilde{K}_{i,j} = \begin{pmatrix} 0 & A \\ -A^T & B \end{pmatrix}. \tag{10.11}$$

Here, the upper-left corner is a zero matrix with dimension $(N_f + g - 1) \times (N_f + g - 1)$. The dimension of the B matrix is $(N_e - N_f - g + 1) \times (N_e - N_f - g + 1)$. Utilizing the Euler characteristic $N_v - N_e + N_f = 2 - 2g$, we find that the dimensions of B are in fact $(N_v + g - 1) \times (N_v + g - 1)$.

If $N_f > N_v$, again, we find that the 0 block is larger than the block of B, and therefore, $\det \tilde{K}^1 = 0$ (see Appendix G for a proof). Because $\{\xi_i\}$ is a compete basis for the edge space, this implies that $\det K^{-1} = 0$, and thus K is a singular matrix.

In summary, we proved that in order to preserve the commutation relations [Eq. (10.6)], we must have $N_v \geqslant N_f$. Otherwise, the K matrix would be singular.

C. Flux attachment and $N_v \leqslant N_f$

Let us now prove that the flux attachment also requires $N_v \leqslant N_f$. Flux attachment implies that for each charge distribution, there is a corresponding unique distribution for magnetic fluxes. Because charge can be distributed on N_v sites, to ensure that there is a corresponding flux distribution for every charge configuration, we must have equal number or more faces to put the fluxes.

A more rigorous proof can be formulated by taking a functional derivative to the generic action (10.1), $\delta S / \delta A_v$, which results in the flux-attachment condition

$$q_v = \frac{k}{2\pi} M_{v,f} \Phi_f. \tag{10.12}$$

If we want the flux attached to a charge to be local (i.e., the flux for a point charge occupies only a single face), for each vertex v, the $M_{v,f}$ is nonzero only for one value of f. As a result, the M matrix defines a mapping from v to f.

This mapping must be injective. Namely, for two different vertices, their corresponding faces must be different. This is so because if two different vertices v and v' are mapped to the same face f, then Eq. (10.12) will require that $q_v = q'_v$, i.e., two different vertices always have the same charge, which is obviously not a physically necessary constraint. Thus, for an injective mapping from vertices to faces, we must have $N_v \leqslant N_f$.

D. Local vertex-surface correspondence

In the previous two subsections we proved that $N_v \leqslant N_f$ and $N_v \geqslant N_f$ must hold simultaneously. Therefore, the graph must have the same numbers of vertices and faces $N_v = N_f$. With $N_v = N_f$, the mapping from vertices to faces discussed above become a one-to-one correspondence between vertices and faces. As addressed in Sec. IX, it is important to ensure that this correspondence is local. As a result, the local vertex-face correspondence arises naturally, when we try to ensure the theory being nonsingular and the key properties of the Chern-Simons gauge theory is preserved.

XI. CHERN-SIMONS GAUGE THEORY ON A TETRAHEDRON

In this section, we demonstrate our generic theory by presenting a specific example, i.e., by discretizing the Chern-Simons gauge theory on a tetrahedron. A tetrahedron is a planar graph defined on a manifold with $g = 0$ (a sphere). In addition, it is easy to verify that a tetrahedron satisfies the criterion presented in Sec. II, and thus a discretized Chern-Simons gauge theory can be constructed. It is also worthwhile to emphasize that a tetrahedron is self-dual (i.e., the dual graph is also a tetrahedron). This is also the simplest setup for discretizing the Chern-Simons gauge theory.

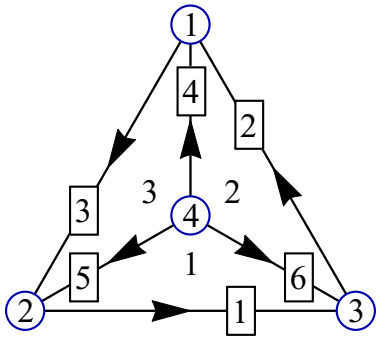

FIG. 10. (Color online) A tetrahedron viewing from the top. The circles represent the vertices, and the arrows are the edges (direction assigned). Here, we label each vertices, edges, and faces using integers. The last face (i.e., the face 4) is on the other side of the tetrahedron invisible from the current view point.

A. The action

We label the vertices, edges, and faces of a tetrahedron as shown in Fig. 10. In this convention, the incident matrix $D_{v,e}$ [Eq. (4.3)] is

$$D = \begin{pmatrix} 0 & +1 & -1 & +1 & 0 & 0 \\ -1 & 0 & +1 & 0 & +1 & 0 \\ +1 & -1 & 0 & 0 & 0 & +1 \\ 0 & 0 & 0 & -1 & -1 & -1 \end{pmatrix} \tag{11.1}$$

and the $\xi_{f,e}$ matrix defined in Eq. (3.6) is

$$\xi = \begin{pmatrix} +1 & 0 & 0 & 0 & +1 & -1 \\ 0 & +1 & 0 & -1 & 0 & +1 \\ 0 & 0 & +1 & +1 & -1 & 0 \\ -1 & -1 & -1 & 0 & 0 & 0 \end{pmatrix}. \tag{11.2}$$

We choose the local vertex-face correspondence such that vertices 1, 2, 3, and 4 pairs up with faces 2, 3, 4, and 1, respectively. Therefore, the $M_{v,f}$ matrix is

$$M = \begin{pmatrix} 0 & 1 & 0 & 0 \\ 0 & 0 & 1 & 0 \\ 0 & 0 & 0 & 1 \\ 1 & 0 & 0 & 0 \end{pmatrix}. \tag{11.3}$$

Using this vertex-face correspondence, we can get the $K_{e,e'}$ matrix following the procedure described in Sec. III B, which is

$$K = \frac{1}{2}\begin{pmatrix} 0 & +1 & +1 & 0 & -1 & -1 \\ -1 & 0 & -1 & +1 & 0 & -1 \\ -1 & +1 & 0 & -1 & +1 & 0 \\ 0 & -1 & +1 & 0 & +1 & -1 \\ +1 & 0 & -1 & -1 & 0 & -1 \\ +1 & +1 & 0 & +1 & +1 & 0 \end{pmatrix}. \tag{11.4}$$

Using these two matrices, the action can be written as shown in Eq. (3.4).

Here, we can verify easily that the K matrix is invertible. In addition, it is straightforward to show that $M^T = M^{-1}$ and $K^T = -K$ (i.e., M is an orthogonal matrix and K is antisymmetric), in agreement with the generic result proved above.

In addition, it is also straightforward to verify that the matrices satisfy the gauge-invariance condition (4.5) because $M\xi = DK^T$.

B. Dual graph

In the dual graph, it is straightforward to get the dual of the incident matrix and that of the ξ matrix:

$$D^* = \begin{pmatrix} +1 & 0 & 0 & 0 & +1 & -1 \\ 0 & +1 & 0 & -1 & 0 & +1 \\ 0 & 0 & +1 & +1 & -1 & 0 \\ -1 & -1 & -1 & 0 & 0 & 0 \end{pmatrix} \tag{11.5}$$

and

$$\xi^* = \begin{pmatrix} 0 & -1 & +1 & -1 & 0 & 0 \\ +1 & 0 & -1 & 0 & -1 & 0 \\ -1 & +1 & 0 & 0 & 0 & -1 \\ 0 & 0 & 0 & +1 & +1 & +1 \end{pmatrix}. \tag{11.6}$$

By comparing the D and ξ^* (ξ and D^*) matrices, we find that $D^* = \xi$ and $\xi^* = -D$, which verify Eqs. (6.1) and (6.2).

In the dual graph, if we use the same vertex-face correspondence, we get the M^* matrix

$$M^* = \begin{pmatrix} 0 & 0 & 0 & 1 \\ 1 & 0 & 0 & 0 \\ 0 & 1 & 0 & 0 \\ 0 & 0 & 1 & 0 \end{pmatrix} \tag{11.7}$$

and the K^* matrix is

$$K^* = \frac{1}{2}\begin{pmatrix} 0 & +1 & +1 & 0 & -1 & -1 \\ -1 & 0 & -1 & +1 & 0 & -1 \\ -1 & +1 & 0 & -1 & +1 & 0 \\ 0 & -1 & +1 & 0 & +1 & -1 \\ +1 & 0 & -1 & -1 & 0 & -1 \\ +1 & +1 & 0 & +1 & +1 & 0 \end{pmatrix}. \tag{11.8}$$

Using the matrices M^*, K^*, and ξ^*, we can write the action for the discretized Chern-Simons gauge theory in the dual graph using Eq. (6.3).

Here, we can verify that $K^* = -K^{-1}$ and $M^* = M^{-1}$, as well as the gauge-invariance condition $M^*\xi^* = D^*(K^*)^T$ [Eq. (6.21)].

XII. CONCLUSIONS AND DISCUSSION

In this paper, we proved that the Chern-Simons gauge theory can be discretized for generic planar graphs on arbitrary 2D closed orientable manifold as long as a local vertex-face correspondence can be defined on the graph. This condition is also necessary if we want the theory to be nonsingular and to preserve some key properties of the Chern-Simons gauge theory. In particular, we showed that the gauge invariance of the discretized theory requires that the vertex-face correspondence to be strictly enforced.

We also find a necessary and sufficient condition, which can be used to determine whether such a correspondence can be defined on a particle graph or not, based on the number of faces and vertices in this graph and its subgraphs.

The generalized discretized Chern-Simons gauge theory that we presented here has a number of interesting applications. One direction of further research is to consider the fractional quantum Hall effect on lattices, a problem that has not attracted much attention so far [22,23]. A more general theory of the fractional quantum Hall effect on lattices is of interest in the context of fractionalized time-reversal breaking topological insulators so far as adiabatic continuity holds [28,30]. These methods are also relevant to frustrated quantum antiferromagnets as we showed recently [12].

There are several open as yet unsolved issues. One is to relax somewhat the vertex-face correspondence. Since, as we showed, this is required by gauge invariance, any violation of this correspondence is equivalent to either the insertion of background static charges or background static fluxes. This viewpoint may offer a way to generalize this construction to other lattices (e.g., triangular and honeycomb) as well as to investigate the role of lattice topological defects such as dislocations and disclinations of time-reversal breaking fluids, including quantum Hall fluids, where the role of geometry has been focus of recent interest [51–60].

As a side comment, it is also worthwhile to note that two of the graphs shown in Fig. 2 (the kagome lattice and the dice lattice) belong to the family of *isostatic lattices*. The terminology of isostatic lattices is developed in the study of mechanical stability transition [61] and, recently, topologically nontrivial elastic modes are observed in some of these isostatic systems, including protected zero-energy edge states, nontrivial topological indices, and topological zero-energy solitons [62–64]. Although the topological nature of those isostatic elastic systems is very different from a Chern-Simons gauge theory, it is not an accident that the same lattices arise in these two seemingly unrelated areas. As shown in Appendix H, the isostatic condition is closely related with (and slightly stronger than) the criterion for the existence of local vertex-face correspondence, which is the fundamental reason why some lattices can be used for both studies.

ACKNOWLEDGMENT

The work was supported in part by the National Science Foundation, under Grants No. PHY-1402971 at the University of Michigan (K.S.) and No. DMR-1408713 at the University of Illinois (E.F.), and by the U. S. Department of Energy, Division of Materials Sciences under Awards No. DE-FG02-07ER46453 and No. DE-SC0012368 through the Frederick Seitz Materials Research Laboratory of the University of Illinois at Urbana-Champaign.

APPENDIX A: SIMPLE GRAPH

Here, we demonstrate the definition of a simple graph by presenting situations that are not allowed in a simple graph, as shown in Fig. 11.

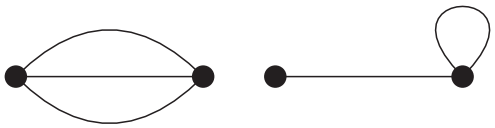

(a) (b)

FIG. 11. Examples of graphs that are not simple. The figures demonstrate situations that are not allowed for a simple graph. (a) Shows a pair of sites connected by three different edges. In (b), one of the edges connects a site with itself (i.e., the two ends of an edge coincide).

APPENDIX B: LOCAL VERTEX-FACE CORRESPONDENCE

In this appendix, we prove that the criterion presented in Sec. II is a sufficient and necessary condition for a graph to have a local vertex-face correspondence by mapping this problem to *Hall's marriage problem* [47].

The *marriage problem* considers a finite set of girls, each of whom knows several boys, and the task is to find the sufficient and necessary condition, under which all the girls can marry the boys in such a way that each girl marries a boy she knows (marriage is assumed to be one-to-one here). The solution to the *marriage problem* lies in *Hall's marriage theorem*, which states that a necessary and sufficient condition for the existence of such a matching is that each set of k girls collectively knows at least k boys.

Our goal here is to identify the sufficient and necessary condition for a graph satisfies the local-flux-attachment condition. This problem can be mapped to the marriage problem by mapping faces into girls and vertices as boys. If the vertex v is the vertex of the face f, the corresponding boy and girl know each other. Under this mapping, the local-flux-attachment condition is exactly the marriage problem.

Here, we first prove that the criterion presented in Sec. II is a necessary condition. We consider a subgraph of G. By mapping to the marriage problem, all the faces in the subgraph form a subset of girls, and the boys that they know are included by the set of vertices of the subgraph, i.e., if the subgraph contains N'_f faces (girls) and N'_v vertices (boys), the number of boys that these girls know is equal to or smaller than N'_v. Therefore, based on *Hall's marriage theorem*, we must have $N'_v \geqslant N'_f$ in every subgraph, if every face can marry a vertex that is adjacent to it. In other words, this criterion is necessary for the existence of a local vertex-face correspondence.

We can also prove that the criterion is sufficient by considering subgraphs that satisfy the following condition: every vertex in the subgraph is adjacent to at least one face of the subgraph. (This condition does not hold for all subgraphs. For example, if a subgraph contains dangling bonds, the vertex located at the free end of a dangling bond is not adjacent to any faces in the subgraph.) For these subgraphs (in which all vertices are adjacent to at least one face of the subgraph), the number of vertices (N'_v) equals to the number of boys that are known by the girls (faces) in the subgraph. Therefore, if the criterion in Sec. II is satisfied, the marriage theorem ensures immediately the existence of (at least) one local vertex-face correspondence.

APPENDIX C: GAUGE SYMMETRY

Here, we prove that Eq. (4.5) is the sufficient and necessary condition to maintain the gauge symmetry in our theory [Eq. (3.4)]. First, we substitute the magnetic flux in Eq. (3.4) by Eq. (3.5):

$$S = \frac{k}{2\pi}\int dt\left(A_v M_{v,f}\xi_{f,e}A_e - \frac{1}{2}A_{e_i}K_{e,e'}\dot{A}_{e'}\right). \tag{C1}$$

Under the gauge transformation

$$A_v \to A_v - \partial_0\phi_v, \tag{C2}$$

$$A_e \to A_e - D_{v,e}\phi_v, \tag{C3}$$

the action (C1) is transferred to

$$\begin{aligned} S \to S + \frac{k}{2\pi}\int dt\Big(&-\dot{\phi}_v M_{v,f}\xi_{f,e}A_e \\ &+\frac{1}{2}D_{v,e}\phi_v K_{e,e'}\dot{A}_{e'} + \frac{1}{2}A_e K_{e,e'}D_{v,e'}\dot{\phi}_v\Big) \\ &-\frac{k}{4\pi}\int dt(D_{v,e}\phi_v K_{e,e'}D_{v',e'}\dot{\phi}_{v'}). \end{aligned} \tag{C4}$$

Here, the second term on the right-hand side is linear in ϕ, while the last term is $O(\phi^2)$. In order to preserve the gauge symmetry, we need both these two terms to vanish, i.e.,

$$\int dt(\dot{\phi}_v M_{v,f}\xi_{f,e}A_e - A_e K_{e,e'}D_{v,e'}\dot{\phi}_v) = 0, \tag{C5}$$

$$\int dt(D_{v,e}\phi_v K_{e,e'}D_{v',e'}\dot{\phi}_{v'}) = 0. \tag{C6}$$

In Eq. (C5), we used the fact that

$$\int dt\; D_{v,e}\phi_v K_{e,e'}\dot{A}_{e'} = \int dt\; A_e K_{e,e'}D_{v,e'}\dot{\phi}_v, \tag{C7}$$

which can be proved via integrating by part and realizing that the K matrix is antisymmetric.

Equations (C5) and (C6) imply that

$$M_{v,f}\xi_{f,e} = K_{e,e'}D_{v,e'}, \tag{C8}$$

$$D_{v,e}K_{e,e'}D_{v',e'} = 0. \tag{C9}$$

These two conditions are not independent to each other. In fact, Eq. (C8) automatically implies Eq. (C9). This can be realized by noticing that according to Eq. (C8), we have

$$D_{v,e}K_{e,e'}D_{v',e'} = D_{v,e}M_{v',f}\xi_{f,e}. \tag{C10}$$

The right-hand side of this equation is zero because $D_{v,e}\xi_{f,e} = 0$, and thus Eq. (C9) arises automatically.

Here, we explain why $D_{v,e}\xi_{f,e} = 0$. For any fixed f, $\xi_{f,e}$ represents a loop in the graph. If v is not a vertex on this loop, $D_{v,e}\xi_{f,e}$ must vanish because $D_{v,e} = 0$. If the loop paths through v, there must be two edges along these loops that are connected to v, which we will call e_1 and e_2. It is easy to realize that according to the definition of ξ and D, $D_{v,e_1}\xi_{f,e_1} = -D_{v,e_2}\xi_{f,e_2}$ (here, we do not sum over repeated indices e_1 and e_2). Therefore, the contributions to $D_{v,e}\xi_{f,e}$ cancel out, i.e., $D_{v,e}\xi_{f,e} = 0$. This relation can also be written in a matrix form and the same is true for the dual graph

$$D\xi^T = D^*(\xi^*)^T = 0, \tag{C11}$$

which will be used below in Appendix E. Here, ξ^T represents the transpose matrix of ξ.

APPENDIX D: DIRECTIONS OF EDGES

In this appendix, we prove that the condition of gauge invariance [Eq. (4.5)] is independent of the choice on the edge directions.

As shown in the main text, we assign a direction for each edge in order to define the vector potential on a graph. These directions can be assigned in arbitrary ways, and the choice of directions will not have any impact for any physics properties. For the condition of gauge invariance [Eq. (4.5)], this statement is also true. To prove this statement, we flip the direction of an arbitrary edge e_0 and consider two different situations: $e_0 = e$ and $e_0 \neq e$.

If $e_0 = e$, as we flip the direction assigned to the edge e_0, the left-hand side of Eq. (4.5) changes sign because $M_{v,f} \to M_{v,f}$ and $\xi_{f,e_0} \to -\xi_{f,e_0}$. The right-hand side of the equation also flips sign since $K_{e_0,e'} \to -K_{e_0,e'}$ and $D_{v,e'} \to D_{v,e'}$. Because both sides of the equation flip sign when we flip the direction of e_0, the equation remains invariant and thus is independent of the choice of the direction of e_0.

If $e \neq e_0$, the left-hand side of Eq. (4.5) remains invariant because neither $M_{v,f}$ nor $\xi_{f,e}$ relies on the direction of e_0. For the right-hand side, because both K_{e,e_0} and $D_{e_0,v}$ flip signs as we flip the direction of e_0, their product remains the same. As a result, the equation is again independent of the direction of e_0.

This conclusion implies that in order to prove Eq. (3.6), it is sufficient to verify the formula for just one specific choice of edge directions.

APPENDIX E: LATTICE DUALITY

In this appendix, we prove that the discretized Chern-Simons theory on the original lattice and the dual lattice are dual to each other by coupling the Chern-Simons gauge theory with gauge fields on the dual lattice

$$S = S_{\mathrm{CS}} + S_{\mathrm{coupling}}. \tag{E1}$$

Here, the first term is our discrete Chern-Simons gauge theory

$$S_{\mathrm{CS}} = \frac{k}{2\pi}\int dt\left(A_v M_{v,f}\Phi_f - \frac{1}{2}A_e K_{e,e'}\dot{A}_{e'}\right) \tag{E2}$$

and the second term couples the Chern-Simons field A with gauge fields on the dual graph a^*

$$\begin{aligned} S_{\mathrm{coupling}} = \int \frac{dt}{2\pi}(&\xi^*_{f^*,e^*}a^*_{e^*}A_v\delta_{f^*,v} + D^*_{v^*,e^*}a^*_{v^*}A_e\delta_{e,e^*} \\ &- \partial_0 a^*_{e^*}A_e\delta_{e,e^*}). \end{aligned} \tag{E3}$$

As will be shown in Appendix E 1, this coupling is gauge invariant.

In Appendix E 1, we first prove that same as in the continuum, the dual gauge field a^* can be used to describe the charge and current on the original lattice and we will also

show that S_{coupling} is gauge invariant. Then, in Appendix E 2, we show that by integrating out the A field, the dual theory is obtained, which matches exactly the discrete Chern-Simons field on the dual lattice (but with a different coupling constant $k^* = -1/k$). Because our action describes a quadratic theory, this calculation is exact.

1. Gauge field on the dual lattice

Same as in the continuum, we can consider the dual gauge field a^* (defined on the dual lattice) as a description for the charge and current on the original lattice. Here, the charge that resides at each vertex is called ρ_v and the current on each edge is labeled as j_e:

$$\rho_v = \frac{1}{2\pi}\xi^*_{f^*,e^*}a^*_{e^*}, \tag{E4}$$

$$j_e = \frac{1}{2\pi}(D^*_{v^*,e^*}a^*_{v^*} - \partial_0 a^*_{e^*}). \tag{E5}$$

In Eq. (E4), we choose $f^* = v$, and for Eq. (E5), $e = e^*$. It is easy to verify that the charge and current are gauge invariant and satisfy the charge conservation law (i.e., the continuity equation)

$$\partial_t \rho_v - D_{v,e} j_e = 0, \tag{E6}$$

where ∂_t is the time derivative and $D_{v,e}$ (the incident matrix) plays the role of a discretized divergence (multiplied by -1).

To prove the gauge invariance, we perform the gauge transformation for a^*:

$$a^*_{v^*} \to a^*_{v^*} - \partial_0 \phi^*_{v^*}, \tag{E7}$$

$$a^*_{e^*} \to a^*_{e^*} - D^*_{v^*,e^*}\phi^*_{v^*}. \tag{E8}$$

Under this transformation, ρ_v and j_e are invariant:

$$\rho_v \to \rho_v - \frac{1}{2\pi}\xi^*_{f^*,e^*}D^*_{v^*,e^*}\phi^*_{v^*} = \rho_v, \tag{E9}$$

$$j_e \to j_e - \frac{1}{2\pi}(D^*_{v^*,e^*}\partial_0\phi^*_{v^*} - \partial_0 D^*_{v^*,e^*}\phi^*_{v^*}) = j_e. \tag{E10}$$

For Eq. (E9), we used the fact $\xi^*_{f^*,e^*}D^*_{v^*,e^*} = 0$. This relation is proved in Eq. (C11) and it is a discretized version of the formula $\nabla \times \nabla = 0$. In Eq. (E10), $D^*_{v^*,e^*}\partial_0\phi^*_{v^*}$ and $-\partial_0 D^*_{v^*,e^*}\phi^*_{v^*}$ cancels out because the incident matrix $D^*_{v^*,e^*}$ is time independent and thus commute with the time derivative ∂_0.

The continuity equation can be proved using the following two equations:

$$\partial_0\rho_v = \frac{1}{2\pi}\xi^*_{v,e^*}\partial_0 a^*_{e^*}, \tag{E11}$$

$$-D_{v,e}j_e = \frac{1}{2\pi}\xi^*_{f^*,e^*}(D^*_{v^*,e^*}a^*_{v^*} - \partial_0 a^*_{e^*}) = -\frac{1}{2\pi}\xi^*_{f^*,e^*}\partial_0 a^*_{e^*}. \tag{E12}$$

In the second equation here, we used the fact that $D_{v,e} = -\xi^*_{f^*,e^*}$ [Eq. (6.2)] and $\xi^*_{f^*,e^*}D^*_{v^*,e^*} = 0$ [Eq. (C11)]. By adding the two questions together, the continuity equation is obtained.

Using Eqs. (E4) and (E5), the coupling between the A and a^* fields [i.e., Eq. (E3)] can be rewritten as

$$S_{\text{coupling}} = \int dt(\rho_v A_v + j_e A_e). \tag{E13}$$

Because both ρ_v and j_e are gauge invariant, the coupling term must also be gauge invariant.

The coupling S_{coupling} is also invariant under gauge transformation

$$A_v \to A_v - \partial_0\phi_v, \tag{E14}$$

$$A_e \to A_e - D_{v,e}\phi_v. \tag{E15}$$

Using Eq. (E13), we find that the gauge transformation turns S_{coupling} into

$$\begin{aligned} S'_{\text{coupling}} &= S_{\text{coupling}} - \int dt(\rho_v\partial_0\phi_v + j_e D_{v,e}\phi_v) \\ &= S_{\text{coupling}} + \int dt(\partial_0\rho_v - j_e D_{v,e})\phi_v. \end{aligned} \tag{E16}$$

After a integration by part (for t), the last term in this formula vanishes due to the continuity equation, and thus S_{coupling} is gauge invariant.

2. Duality transformation

In the path-integral approach, a gauge-fixing term $S_{\text{gaugefixing}}$ needs to be introduced

$$S = S_{\text{CS}} + S_{\text{coupling}} + S_{\text{gaugefixing}}. \tag{E17}$$

Without loss of generality, here we choose

$$S_{\text{gaugefixing}} = \frac{\alpha}{2}\int \frac{dt}{2\pi}\left(\frac{dA_v}{dt}\frac{dA_v}{dt}\right). \tag{E18}$$

In the frequency space, the action of Eq. (E17) takes the following form:

$$S = S_{\text{CS}} + S_{\text{coupling}} + S_{\text{gaugefixing}} \tag{E19}$$

$$\begin{aligned} &= \frac{k}{2}\sum_{\omega}(\mathbf{A_v}(\omega) \quad \mathbf{A_e}(\omega))\begin{pmatrix}\alpha\omega^2/k & M\xi \\ (M\xi)^T & -i\omega K\end{pmatrix}\begin{pmatrix}\mathbf{A_v}(-\omega) \\ \mathbf{A_e}(-\omega)\end{pmatrix} \\ &\quad + \sum_{\omega}(\mathbf{a^*_{v^*}}(\omega) \quad \mathbf{a^*_{e^*}}(\omega))\begin{pmatrix}0 & D^* \\ (\xi^*)^T & i\omega\end{pmatrix}\begin{pmatrix}\mathbf{A_v}(-\omega) \\ \mathbf{A_e}(-\omega)\end{pmatrix}. \end{aligned} \tag{E20}$$

Here, we write the Lagrangian as block matrices. Bold letters in this equation are vectors. For example, $\mathbf{a^*_{e^*}}$ represents an N_{e^*}-dimensional vector, whose components are $a^*_{e^*}$ on each

edge. The same is true for $\mathbf{a}^*_{\mathbf{v}^*}$, $\mathbf{A}_\mathbf{e}$, or $\mathbf{A}_\mathbf{v}$. The first matrix in the equation above contains $S_{\rm CS}$ and $S_{\rm gaugefixing}$, while the second matrix is for $S_{\rm coupling}$.

By integrating out the A field, we obtain a dual gauge theory for a^* on the dual graph. For a quadratic theory as shown above, this can be done exactly

$$S=-\frac{1}{2k}\sum_\omega (\mathbf{a}^*_{\mathbf{v}^*}(\omega)\quad \mathbf{a}^*_{\mathbf{e}^*}(\omega))\begin{pmatrix}0 & D^*\\ (\xi^*)^T & i\omega\end{pmatrix}\begin{pmatrix}\alpha\omega^2/k & M\xi\\ (M\xi)^T & -i\omega K\end{pmatrix}^{-1}\begin{pmatrix}0 & \xi^*\\ (D^*)^T & -i\omega\end{pmatrix}\begin{pmatrix}\mathbf{a}^*_{\mathbf{v}^*}(-\omega)\\ \mathbf{a}^*_{\mathbf{e}^*}(-\omega)\end{pmatrix}. \tag{E21}$$

The inverse matrix in the equation above can be computed using the technique of *blockwise inversion*

$$\begin{pmatrix}A & B\\ C & D\end{pmatrix}^{-1}=\begin{pmatrix}(A-BD^{-1}C)^{-1} & -(A-BD^{-1}C)^{-1}BD^{-1}\\ -D^{-1}C(A-BD^{-1}C)^{-1} & D^{-1}+D^{-1}C(A-BD^{-1}C)^{-1}BD^{-1}\end{pmatrix}, \tag{E22}$$

where A, B, C, and D are matrix subblocks. For our matrix inverse, the block A is an identity matrix (multiply by a real number $\alpha\omega^2/k$), and we have $B=C^T=M\xi$ and the block D is $-i\omega K$. Using the commutation relation (7.10) and the fact that this commutator is zero for two contractible loops, it is easy to show that

$$\xi(K)^{-1}(\xi)^T=0, \tag{E23}$$

i.e., $BD^{-1}C=0$. Therefore, we find that

$$\begin{pmatrix}\alpha\omega^2/k & M\xi\\ (M\xi)^T & -i\omega K\end{pmatrix}^{-1}=\begin{pmatrix}\frac{k}{\alpha\omega^2} & -\frac{ik}{\alpha\omega^3}M\xi K^{-1}\\ -\frac{ik}{\alpha\omega^3}K^{-1}\xi^T M^T & -\frac{1}{i\omega}K^{-1}-\frac{k}{\alpha\omega^4}K^{-1}\xi^T M^T M\xi K^{-1}\end{pmatrix}. \tag{E24}$$

Now, we will use Eq. (6.20), which tells that

$$M\xi K^{-1}=-D=\xi^*, \tag{E25}$$

$$K^{-1}\xi^T M^T=D^T=-(\xi^*)^T. \tag{E26}$$

Here, we also used the fact that K is an antisymmetric matrix and Eq. (6.2) ($D=-\xi^*$). Using these two relations, we find that

$$\begin{pmatrix}\alpha\omega^2/k & M\xi\\ (M\xi)^T & -i\omega K\end{pmatrix}^{-1}=\begin{pmatrix}\frac{k}{\alpha\omega^2} & -\frac{ik}{\alpha\omega^3}\xi^*\\ \frac{ik}{\alpha\omega^3}(\xi^*)^T & -\frac{1}{i\omega}K^{-1}+\frac{k}{\alpha\omega^4}(\xi^*)^T\xi^*\end{pmatrix}. \tag{E27}$$

Therefore,

$$\begin{aligned}S=&-\frac{1}{2k}\sum_\omega (\mathbf{a}^*_{\mathbf{v}^*}(\omega)\quad \mathbf{a}^*_{\mathbf{e}^*}(\omega))\begin{pmatrix}0 & D^*\\ (\xi^*)^T & i\omega\end{pmatrix}\begin{pmatrix}\frac{k}{\alpha\omega^2} & -\frac{ik}{\alpha\omega^3}\xi^*\\ \frac{ik}{\alpha\omega^3}(\xi^*)^T & -\frac{1}{i\omega}K^{-1}+\frac{k}{\alpha\omega^4}(\xi^*)^T\xi^*\end{pmatrix}\begin{pmatrix}0 & \xi^*\\ (D^*)^T & -i\omega\end{pmatrix}\begin{pmatrix}\mathbf{a}^*_{\mathbf{v}^*}(-\omega)\\ \mathbf{a}^*_{\mathbf{e}^*}(-\omega)\end{pmatrix}\\ =&-\frac{1}{2k}\sum_\omega (\mathbf{a}^*_{\mathbf{v}^*}(\omega)\quad \mathbf{a}^*_{\mathbf{e}^*}(\omega))\begin{pmatrix}0 & -\frac{1}{i\omega}D^*K^{-1}\\ 0 & -K^{-1}\end{pmatrix}\begin{pmatrix}0 & \xi^*\\ (D^*)^T & -i\omega\end{pmatrix}\begin{pmatrix}\mathbf{a}^*_{\mathbf{v}^*}(-\omega)\\ \mathbf{a}^*_{\mathbf{e}^*}(-\omega)\end{pmatrix}\\ =&-\frac{1}{2k}\sum_\omega (\mathbf{a}^*_{\mathbf{v}^*}(\omega)\quad \mathbf{a}^*_{\mathbf{e}^*}(\omega))\begin{pmatrix}0 & D^*K^{-1}\\ -K^{-1}(D^*)^T & i\omega K^{-1}\end{pmatrix}\begin{pmatrix}\mathbf{a}^*_{\mathbf{v}^*}(-\omega)\\ \mathbf{a}^*_{\mathbf{e}^*}(-\omega)\end{pmatrix}.\end{aligned} \tag{E28}$$

Here, we used the fact that $D^*(\xi^*)^T=0$ [Eq. (C11)] and $D^*K^{-1}(D^*)^T=\xi K^{-1}\xi^T=0$ [Eqs. (6.1) and (E23)].

Because $K^{-1}=-K^*$ and $D^*K^*=-M^*\xi^*$, we get

$$\begin{aligned}S=&-\frac{1}{2k}\sum_\omega (\mathbf{a}^*_{\mathbf{v}^*}(\omega)\quad \mathbf{a}^*_{\mathbf{e}^*}(\omega))\begin{pmatrix}0 & -D^*K^*\\ -(D^*K^*)^T & -i\omega K^*\end{pmatrix}\begin{pmatrix}\mathbf{a}^*_{\mathbf{v}^*}(-\omega)\\ \mathbf{a}^*_{\mathbf{e}^*}(-\omega)\end{pmatrix}\\ =&-\frac{1}{2k}\sum_\omega (\mathbf{a}^*_{\mathbf{v}^*}(\omega)\quad \mathbf{a}^*_{\mathbf{e}^*}(\omega))\begin{pmatrix}0 & M^*\xi^*\\ (M^*\xi^*)^T & -i\omega K^*\end{pmatrix}\begin{pmatrix}\mathbf{a}^*_{\mathbf{v}^*}(-\omega)\\ \mathbf{a}^*_{\mathbf{e}^*}(-\omega)\end{pmatrix}.\end{aligned} \tag{E29}$$

By transferring from the frequency space ω back to time t, we find

$$S=\frac{-1/k}{2\pi}\int dt\left(a^*_{v^*}M^*_{v^*,f^*}\Phi^*_{f^*}-\frac{1}{2}a^*_{e^*}K^*_{e^*,e'^*}\dot{a}^*_{e'^*}\right). \tag{E30}$$

This is exactly our discrete Chern-Simons gauge theory defined on the dual graph [Eq. (6.3)] with topological index $k^*=-1/k$.

APPENDIX F: EDGE SPACE, CIRCUIT SUBSPACE, AND THE CUT SUBSPACE

In this section, we prove that the edge space is the direct sum of the circuit subspace and the cut subspace. Although this conclusion applies generically to planar and nonplanar graphs, we will only discuss planar graphs here for simplicity since the paper only considers planar ones.

We first prove that the circuit subspace and the cut subspace are orthogonal to each other. This can be verified easily by noticing that vectors from these two spaces (ξ_C and ξ_H) are orthogonal to each other (i.e., their dot product is zero):

$$\xi_{C,e},\xi_{H,e} = 0. \tag{F1}$$

In addition, we can prove that the dimension of the circuit subspace plus the dimension of the cut subspace coincides with the dimension of the edge space. Combined with the orthogonality proved above, this conclusion implies that the direct sum of the circuit subspace and the cut subspace is the edge space.

As mentioned in the main text, the basis of the circuit subspace can be formed by all independent (contractible and noncontractible) cycles of a graph. For a planar graph with N_f faces defined on a manifold with genus g, there are $N_f - 1$ independent contractible cycles and $2g$ independent noncontractible cycles, i.e., $N_f - 1 + 2g$ independent loops in total. Therefore, the dimensionality of the of circuit subspace is $N_f - 1 + 2g$.

For a planar graph G, cut sets correspond to contractible cycles in the dual graph G^*. Because the dual graph has N_v faces, same as the number of vertices in the original graph, the number of independent cut sets (i.e., the number of independent contractible cycles in the dual graph) is $N_v - 1$.

If we add the dimensions of the cut subspace and the circuit subspace together, we get $N_f + N_v - 2 + 2g$, which coincides with the number of edges N_e, i.e., the dimension of the edge space. Here, we utilized the fact that a closed orientable surface with genus g, the Euler characteristic is $2 - 2g$:

$$N_v - N_e + N_f = 2 - 2g. \tag{F2}$$

Because the circuit subspace and the cut subspace are two orthogonal subspaces of the edge space, and the total dimensions of these two subspaces match the dimensions of the edge space, we proved that the direct sum of these two subspaces is the edge space.

APPENDIX G: DETERMINANT OF A BLOCK MATRIX

Here, we consider a $(N + M) \times (N + M)$ matrix

$$\mathcal{M} = \begin{pmatrix} 0 & C \\ D & B \end{pmatrix}, \tag{G1}$$

where each letter in the matrix represents a block matrix and the 0 (B) matrix has dimensions $N \times N$ ($M \times M$). We will prove below that the determinant of this matrix is zero when the size of the 0 block is larger than the B block (i.e., $N > M$).

First, we define a set of $N + M$ vectors $e_i = (0,0,\ldots,1,\ldots,0)$, such that only the ith component of the vector e_i is nonzero, while $i = 1,2,\ldots,N + M$. Here, these vectors span a $N + M$-dimensional linear space. This linear space is the direct sum of two subspaces $V_1 \oplus V_2$, where V_1 is spanned by the vectors e_i with $1 \leqslant i \leqslant N$ and V_2 by those with $N + 1 \leqslant i \leqslant N + M$, and it is easy to check that V_1 and V_2 are orthogonal to each other.

Because the upper-left block of the matrix only contains zeros, $e_i \mathcal{M} e_j = 0$ for $i \leqslant N$ and $j \leqslant N$. It implies that for any vector e_j with $j \leqslant N$, the vector $\mathcal{M}e_j$ is orthogonal to any vectors in the subspace V_1. In other words, $\mathcal{M}e_j$ is a vector in the subspace V_2. For $j = 1,2,\ldots,N$, $\mathcal{M}e_j$ generates N vectors in the space of V_2. If $N > M$, some of these N vectors must be linearly dependent because the space V_2 can only have M independent vectors. Therefore, we can construct (at least) one zero vector using these N vectors $\mathcal{M}e_j$:

$$\sum_{j=1}^{N} a_j \mathcal{M} e_j = 0, \tag{G2}$$

where a^j are N numbers. This implies immediately that the $\mathcal{M}$ matrix has (at least) one null vector $v = \sum_{j=1}^{N} a_j e_j$:

$$\mathcal{M}v = \sum_{j=1}^{N} \mathcal{M} a_j e_j = 0. \tag{G3}$$

Having a zero eigenvalue implies that the determinant of $\mathcal{M}$ must be zero.

APPENDIX H: ISOSTATIC CONDITION, ELASTICITY, AND LOCAL VERTEX-FACE CORRESPONDENCE

In this appendix, we reveal the connection between the isostatic condition and the criterion for the existence of a local vertex-face correspondence. The idea of isostaticity plays an important role in the study of mechanics stability. It comes from the counting argument developed by Maxwell [61]. If we construct an elastic system by connecting beads with rigid rods (and allow the rods to rotate freely around each joint), the rigidity of the system can be determined by comparing the total number of constraints and the total number of degrees of freedom. In 2D, the total number of degrees here is two times the number of beads because each bead has two degrees of freedom in 2D, while the number of constraints is the number of rods since each rod enforces one constraint by fixing the distance between two beads. If we consider such a system as a graph (i.e., beads as vertices and rods as edges), the number of degrees of freedom is $2N_v$, while the number of constraints is N_e. The isostatic condition requires these two numbers to coincide. If all the constraints are independent (i.e., no redundancy), this condition represents the verge of a mechanical stability (i.e., a phase transition point). If we add/remove one edge (rod) to the system, the system becomes stable/floppy. The rigorous formula for the isostatic condition in 2D is

$$2N_v = N_e + 3. \tag{H1}$$

Here, an extra number 3 is introduced to the right-hand side to represent the trivial global degrees of freedom (two translations and one rotation), which will always arise. Using the Euler characteristic ($N_v - N_e + N_f = 2 - 2g$), we can rewrite the

isostatic condition as

$$N_v = N_f + 1 + 2g, \tag{H2}$$

where g is the genus of the underlying manifold. In the thermal dynamic limit ($N_v \to \infty$ and $N_f \to \infty$), we can ignore the finite part $1 + 2g$ and, therefore, the condition coincides with our requirement of $N_v = N_f$.

In addition, for an isostatic system, to ensure that there are no redundant constraints, one shall require that for any subsystem (subgraph), the total number of degrees of freedom always exceeds (or is equal to) the number of constraints (plus three):

$$2N_v' \geqslant N_e' + 3, \tag{H3}$$

where N_v' and N_e' are number of vertices and edges in a subgraph, while 3 on the right-hand side comes from global translations and rotations. If a subgraph has the topology of a disk (i.e., the Euler characteristic is $N_v - N_e + N_f = 1$), we can rewrite the condition as

$$N_v' \geqslant N_f' + 2, \tag{H4}$$

which is very similar to but slightly stronger than our criterion of local vertex-face correspondence ($N_v' \geqslant N_f'$).

Because our criterion is slightly weaker, some of the lattices/graphs that are not isostatic can still be used to construct a discretized Chern-Simons gauge theory, e.g., Fig. 2(d).

[1] E. Witten, Commun. Math. Phys. **121**, 351 (1989).
[2] S. Deser, R. Jackiw, and S. Templeton, Phys. Rev. Lett. **48**, 975 (1982).
[3] S. C. Zhang, T. H. Hansson, and S. Kivelson, Phys. Rev. Lett. **62**, 82 (1989).
[4] A. López and E. Fradkin, Phys. Rev. B **44**, 5246 (1991).
[5] X. G. Wen, Adv. Phys. **44**, 405 (1995).
[6] Y.-H. Chen, F. Wilczek, E. Witten, and B. I. Halperin, Int. J. Mod. Phys. B **3**, 1001 (1989).
[7] X. G. Wen, F. Wilczek, and A. Zee, Phys. Rev. B **39**, 11413 (1989).
[8] E. Fradkin, *Field Theories of Condensed Matter Physics,* 2nd ed. (Cambridge University Press, Cambridge, UK, 2013).
[9] E. Fradkin, Phys. Rev. Lett. **63**, 322 (1989).
[10] D. Eliezer and G. W. Semenoff, Phys. Lett. B **286**, 118 (1992).
[11] D. Eliezer and G. W. Semenoff, Ann. Phys. (NY) **217**, 66 (1992).
[12] K. Kumar, K. Sun, and E. Fradkin, Phys. Rev. B **90**, 174409 (2014).
[13] K. Yang, L. K. Warman, and S. M. Girvin, Phys. Rev. Lett. **70**, 2641 (1993).
[14] G. Misguich, T. Jolicoeur, and S. M. Girvin, Phys. Rev. Lett. **87**, 097203 (2001).
[15] A. López, A. G. Rojo, and E. Fradkin, Phys. Rev. B **49**, 15139 (1994).
[16] E. Tang, J.-W. Mei, and X.-G. Wen, Phys. Rev. Lett. **106**, 236802 (2011).
[17] K. Sun, Z. Gu, H. Katsura, and S. Das Sarma, Phys. Rev. Lett. **106**, 236803 (2011).
[18] T. Neupert, L. Santos, C. Chamon, and C. Mudry, Phys. Rev. Lett. **106**, 236804 (2011).
[19] D. N. Sheng, Z.-C. Gu, K. Sun, and L. Sheng, Nat. Commun. **2**, 389 (2011).
[20] N. Regnault and B. A. Bernevig, Phys. Rev. X **1**, 021014 (2011).
[21] S. A. Parameswaran, R. Roy, and S. L. Sondhi, C. R. Phys. **14**, 816 (2013).
[22] A. Kol and N. Read, Phys. Rev. B **48**, 8890 (1993).
[23] G. Möller and N. R. Cooper, Phys. Rev. Lett. **103**, 105303 (2009).
[24] A. S. Sørensen, E. Demler, and M. D. Lukin, Phys. Rev. Lett. **94**, 086803 (2005).
[25] R. N. Palmer and D. Jaksch, Phys. Rev. Lett. **96**, 180407 (2006).
[26] M. Hafezi, A. S. Sørensen, E. Demler, and M. D. Lukin, Phys. Rev. A **76**, 023613 (2007).
[27] R. N. Palmer, A. Klein, and D. Jaksch, Phys. Rev. A **78**, 013609 (2008).
[28] Y.-H. Wu, J. K. Jain, and K. Sun, Phys. Rev. B **86**, 165129 (2012).
[29] T. Scaffidi and G. Möller, Phys. Rev. Lett. **109**, 246805 (2012).
[30] Y.-H. Wu, J. K. Jain, and K. Sun, Phys. Rev. B **91**, 041119 (2015).
[31] X.-L. Qi, T. L. Hughes, and S.-C. Zhang, Phys. Rev. B **78**, 195424 (2008).
[32] G. Y. Cho and J. E. Moore, Ann. Phys. (NY) **326**, 1515 (2011).
[33] A. M. Chan, T. L. Hughes, S. Ryu, and E. Fradkin, Phys. Rev. B **87**, 085132 (2013).
[34] T. H. Hansson, T. Kvorning, V. P. Nair, and G. J. Sreejith, Phys. Rev. B **91**, 075116 (2015).
[35] Y. You and E. Fradkin, Phys. Rev. B **88**, 235124 (2013).
[36] G. Murthy and R. Shankar, arXiv:1108.5501.
[37] G. Murthy and R. Shankar, Phys. Rev. B **86**, 195146 (2012).
[38] For 2D orientable surfaces in 3D Euclidean space, an orientation can be chosen using the right-hand rule to define a "clockwise" direction for loops in the surface. This orientation (i.e., clockwise or counterclockwise) cannot be globally defined for nonorientable surfaces, e.g., a Möbius stripe. For the Chern-Simons gauge theory, orientation is required, and thus we only study orientable surfaces.
[39] K. G. Wilson, Phys. Rev. D **10**, 2445 (1974).
[40] J. Kogut and L. Susskind, Phys. Rev. D **11**, 395 (1975).
[41] J. B. Kogut, Rev. Mod. Phys. **51**, 659 (1979).
[42] M. Creutz, *Quarks, Gluons and Lattices* (Cambridge University Press, Cambridge, UK, 1983).
[43] R. Kantor and L. Susskind, Nucl. Phys. B **366**, 533 (1991).
[44] J. Fröhlich and P. Marchetti, Commun. Math. Phys. **121**, 177 (1989).
[45] P. A. M. Dirac, *Lectures in Quantum Field Theory* (Academic, New York, 1966).
[46] X.-G. Wen, Int. J. Mod. Phys. B **4**, 239 (1990).
[47] R. J. Wilson, *Introduction to Graph Theory* (Longman, London, 1998).
[48] N. Biggs, *Algebraic Graph Theory* (Cambridge University Press, Cambridge, UK, 1974).
[49] C.-H. Tze, Int. J. Mod. Phys. A **3**, 1959 (1988).
[50] A. M. Polyakov, Mod. Phys. Lett. A **3**, 325 (1988).

[51] N. Read, Phys. Rev. B **79**, 045308 (2009).
[52] T. L. Hughes, R. G. Leigh, and E. Fradkin, Phys. Rev. Lett. **107**, 075502 (2011).
[53] B. Bradlyn, M. Goldstein, and N. Read, Phys. Rev. B **86**, 245309 (2012).
[54] T. L. Hughes, R. G. Leigh, and O. Parrikar, Phys. Rev. D **88**, 025040 (2013).
[55] G. Y. Cho, Y. You, and E. Fradkin, Phys. Rev. B **90**, 115139 (2014).
[56] Y. You, G. Y. Cho, and E. Fradkin, Phys. Rev. X **4**, 041050 (2014).
[57] M. Fremling, T. H. Hansson, and J. Suorsa, Phys. Rev. B **89**, 125303 (2014).
[58] B. Bradlyn and N. Read, Phys. Rev. B **91**, 165306 (2015).
[59] A. Gromov, G. Y. Cho, Y. You, A. G. Abanov, and E. Fradkin, Phys. Rev. Lett. **114**, 016805 (2015)
[60] M. Geracie, D. T. Son, C. Wu, and S.-F. Wu, Phys. Rev. D **91**, 045030 (2015).
[61] J. C. Maxwell, Philos. Mag. **27**, 294 (1865).
[62] K. Sun, A. Souslov, X. Mao, and T. C. Lubensky, Proc. Natl. Acad. Sci. USA **109**, 12369 (2012).
[63] C. L. Kane and T. C. Lubensky, Nat. Phys. **10**, 39 (2014).
[64] B. G.-g. Chen, N. Upadhyaya, and V. Vitelli, Proc. Natl. Acad. Sci. USA **111**, 13004 (2014).